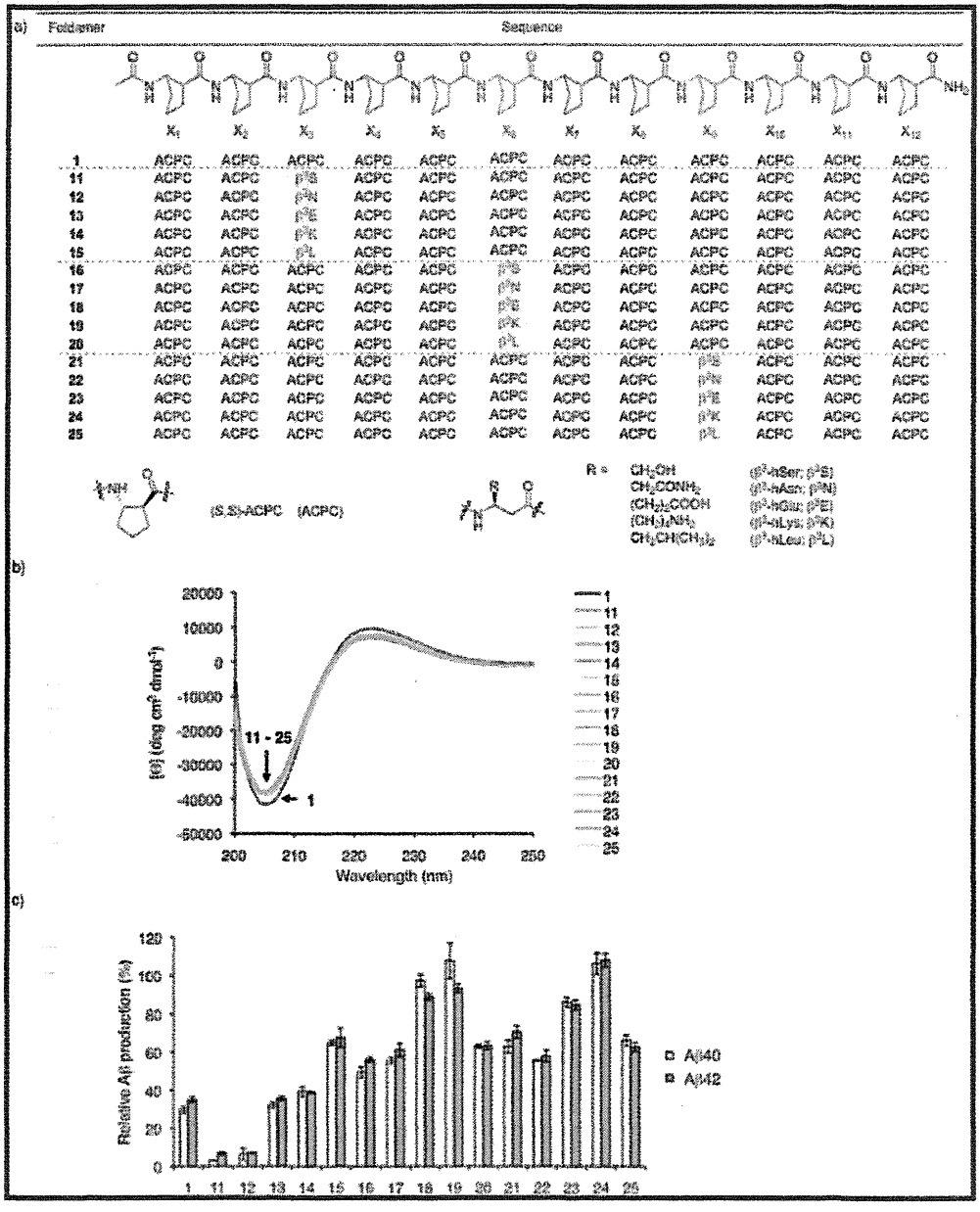

Figure 5. Structure, CD spectra, and γ-secretase-inhibitory activity of foldamers **11**–**25**. (a) Chemical structure. (b) CD spectra in methanol. The molar ellipticity [Θ] values have been normalized for oligomer concentration and the number of backbone amide groups. (c) Inhibition of γ-secretase activity by foldamers at 100 nM in an in vitro assay (n = 3).

5c).[31] Most foldamers exhibited γ-secretase-inhibitory activity; foldamers **11** (X_3 = β^3-hSer) and **12** (X_3 = β^3-hAsn) showed much stronger activity than the parent foldamer **1**, while the other foldamers showed comparable or weaker activity. In general, substitution at X_3 (foldamers **11**–**15**) tended to increase the inhibitory activity, while substitution at position X_6 (foldamers **16**–**20**) or X_9 (foldamers **21**–**25**) tended to decrease it. The activity of foldamers with charged residues (β^3-hGlu; **18** and **23**, β^3-hLys; **19** and **24**) at position X_6 or X_9 was greatly reduced, although substitution at X_3 had only a minimal effect (**13** and **14**). This is consistent with the hypothesis that the foldamers are recognized by γ-secretase as transmembrane mimetics via hydrophobic interaction at the initial substrate docking site. Thus, charged residues at position X_6 or X_9 would be inappropriate for the interaction. In the case of β^3-hLeu, the inhibitory activity was moderately reduced, and the effect was independent of the substitution position (**15**, **20**, **25**).

Among foldamers **11**–**25**, **11** and **12**, which contain β^3-hSer and β^3-hAsn, respectively, showed potent inhibitory activity. This result suggests that a neutral and hydrophilic functional group at X_3 is preferable for strong γ-secretase inhibition. Thus, we designed and synthesized foldamers **26**–**34**, which contain β^3-hThr, β^3-hTyr, β^3-hGln at positions X_3, X_6, and X_9 (Figure 6a). As shown in Figure 6b, the CD spectra of these foldamers were similar to those of foldamers **11**–**25** and are characteristic of a right-handed 12-helix. The signal intensities were very

dx.doi.org/10.1021/jm301306c | J. Med. Chem. 2013, 56, 1443–1454

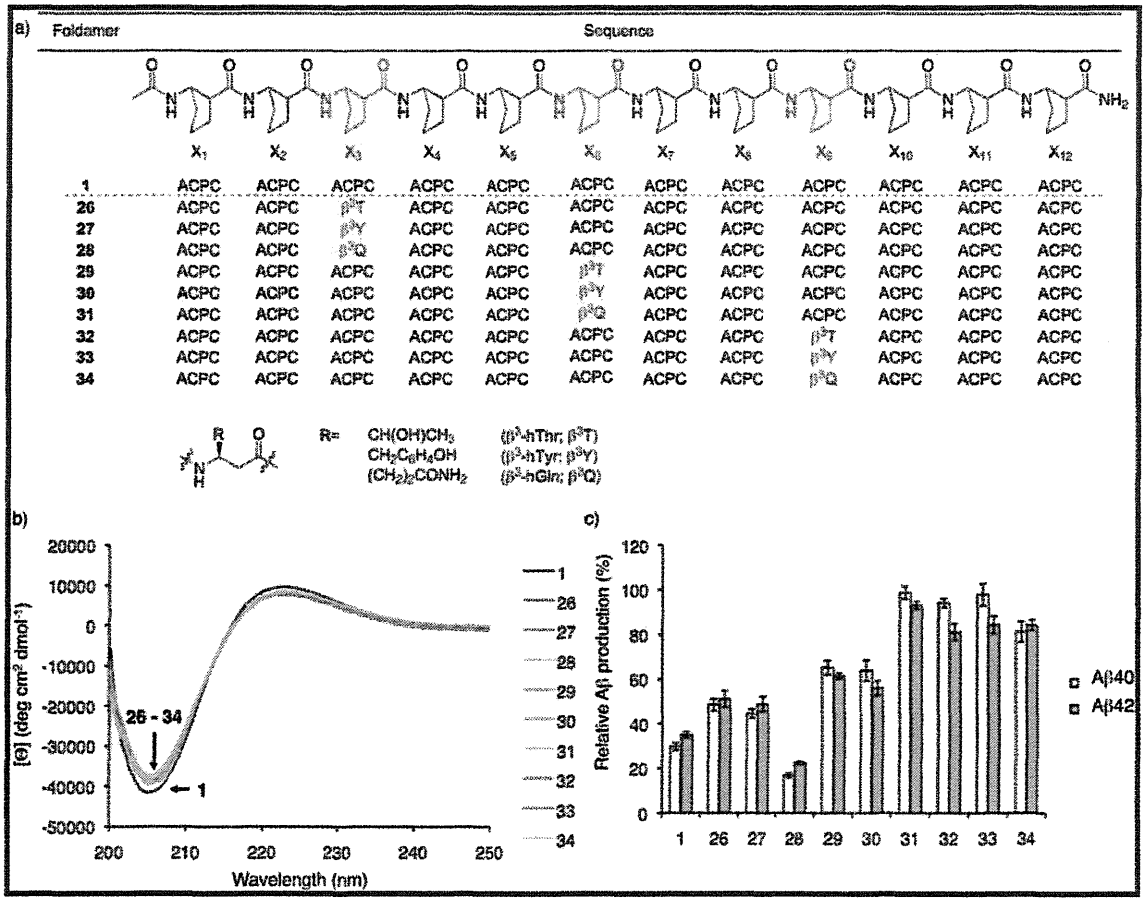

Figure 6. Structure, CD spectra, and γ-secretase-inhibitory activity of foldamers **26**–**34**. (a) Chemical structure. (b) CD spectra in methanol. The molar ellipticity [Θ] values have been normalized for oligomer concentration and the number of backbone amide groups. (c) Inhibition of γ-secretase activity by foldamers at 100 nM in an in vitro assay (n = 3).

similar, suggesting that the foldamers **11**–**34** have similar populations of 12-helix. The inhibitory potency of foldamers **26**–**34** at 100 nM was measured by means of in vitro assay using recombinant substrate (Figure 6c).[31] Most of the foldamers showed weaker γ-secretase-inhibitory activity than the parent foldamer **1** except for **28** (X_3 = β^3-hGln). Modification at the X_3 position with β^3-hGln resulted in relatively potent activity. Both **28** and **12** (X_3 = β^3-hAsn) contain a carboxamide functional group, suggesting that the presence of a neutral and hydrophilic carboxamide group is important for the activity. Further, **12** showed stronger activity than **28**, which may suggest that a smaller side chain group is favorable for the inhibitory activity. Despite the similarity of the β^3-hThr and β^3-hSer side chain functional groups, foldamer **26** (X_3 = β^3-hThr) showed only modest γ-secretase-inhibitory activity, while foldamer **11** (X_3 = β^3-hSer) showed potent activity. The additional methyl group in the β^3-hThr side chain might cause steric repulsion at the interface of γ-secretase. This result also suggests that a smaller functionality is preferable for effective inhibition of γ-secretase activity.

In order to clarify the best position for modification, we have synthesized foldamers **35**–**42** with the replacement of ACPC with β^3-hSer or β^3-hAsn on positions X_1, X_2, X_4, X_5 (Figure 7a). As shown in Figure 7b, the CD spectra of these foldamers were similar to those of foldamers **11**–**34** and are characteristic of a right-handed 12-helix. The inhibitory potency of foldamers **35**–**42**, along with **11** and **12**, was measured at 100 nM (Figure 7c). Foldamers **11** and **12**, which contain β^3-hSer and β^3-hAsn at position X_3, respectively, showed potent inhibitory activity. This result confirmed that the X_3 position is the most favorable position to modify.

Since the X_3 position seemed appropriate for modification, we further designed and synthesized four additional foldamers with substitution at X_3 (**43**–**46**, Figure 8a). β-Amino acids with a relatively small functional group were chosen. β^3-hCys was selected for **43**, since the thiol group is polar, though it is prone to be oxidized. Also, a hydrophilic ring-constrained β-amino acid, Fmoc-*trans*-4-aminotetrahydrofuran-3-carboxylic acid ((*R*,*R*)-AFC),[49] was selected in anticipation of both hydrophilicity and strong induction of 12-helical structure. In addition, we chose β^3-hGly and β^3-hAla, which have no side chain functional group and a methyl side chain functional group, respectively. Glycine and alanine are small residues frequently found at the contact interfaces between transmembrane helices.[50] The foldamers **43**–**46** were synthesized and purified in the same manner. The synthesis of Fmoc-(*R*,*R*)-AFC-OH is described in Supporting Information.[49]

Foldamers **43**–**46** each formed a stable 12-helix in methanol, as demonstrated by the CD spectra; the intensities at 222 nm were quite similar to those of foldamers **11**–**42** except for **44**

dx.doi.org/10.1021/jm301306c | J. Med. Chem. 2013, 56, 1443–1454

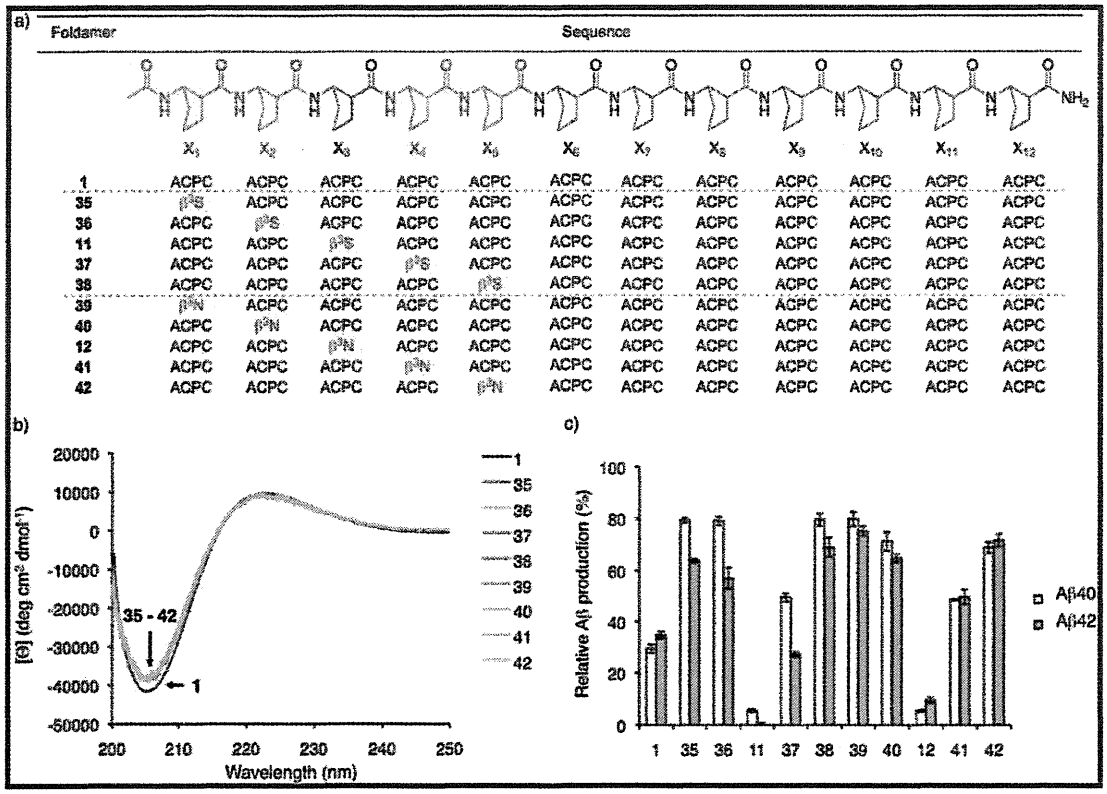

Figure 7. Structure, CD spectra, and γ-secretase-inhibitory activity of foldamers **35**–**42**. (a) Chemical structure. (b) CD spectra in methanol. The molar ellipticity [Θ] values have been normalized for oligomer concentration and the number of backbone amide groups. (c) Inhibition of γ-secretase activity by foldamers at 100 nM in an in vitro assay (n = 3).

(Figure 8b). As expected, foldamer **44** showed strong CD intensity comparable to that of foldamer **1**, suggesting that its 12-helix conformation is more stable than those of the other modified foldamers. The inhibitory potency of foldamers **43**–**46** at 100 nM was measured by means of in vitro assay (Figure 8c). All the foldamers showed potent γ-secretase-inhibitory activity comparable to or even stronger than that of foldamer **1**. Interestingly, foldamers **45** (X_3 = β^3-hGly) and **46** (X_3 = β^3-hAla) showed slightly more potent activity than foldamer **1**, even though the population of 12-helix was decreased and they contain no polar side chain. This result indicates that a small functional group at the X_3 position is superior to ACPC in terms of efficient inhibition of γ-secretase.

In order to clarify the inhibitory potency more precisely, the IC_{50} values of potent foldamers were measured using an in vitro assay. Foldamers **11** (X_3 = β^3-hSer), **12** (X_3 = β^3-hAsn), and **45** (X_3 = β^3-hGly) were selected from the initial screening. As shown in Table 3, foldamers **11** and **12** were the most potent inhibitors; they showed similar IC_{50} values and were more than 10-fold more potent than the lead foldamer **1**. Foldamer **45** showed weaker inhibitory activity but was still more potent than foldamer **1**. The IC_{50} values for foldamer **1** were slightly different from the values reported previously.[12] We have experienced that IC_{50} is somewhat varied (75–150%) using a different lot of the recombinant substrate for in vitro assay by unknown reason. However, the difference in the potency of modified peptides compared to that of foldamer **1** is almost similar. To make adequate comparison throughout the manuscript, we have shown exact values of IC_{50}.

Next, the inhibitory activity of the potent foldamers was measured using a cell-based assay. As noted previously, there is serious concern about adverse effects caused by GSIs that inhibit the release of NICD, a signaling molecule in the Notch pathway.[3−7] Thus, a means to spare Notch-cleaving γ-secretase activity is considered mandatory for development of AD therapeutics. We established a HEK293-based reporter cell line stably expressing APP carrying the Swedish mutation, truncated notch, notch intracellular domain (NICD) driven TP1-firefly luciferase, and EGFP (NLNTK cell line).[51] Secretion of Aβ from NLNTK cells in the presence of foldamers **1**, **11**, and **12** was quantified by ELISA. Simultaneously, notch cleavage was evaluated in terms of firefly luciferase activity in NLNTK cells. As shown in Table 4, foldamers **11** (X_3 = β^3-hSer) and **12** (X_3 = β^3-hAsn) showed greater activity than foldamer **1** (X_3 = ACPC). Both foldamers **11** and **12** contain a side chain functional group capable of hydrogen bond formation. The hydrogen bond donating nature might be important for their potent activities. Foldamer **1** preferentially inhibited NICD over Aβ production in NLNTK cells, which is a different selectivity from that which we found previously.[12] This difference is probably due to the difference of assay method and cell type. Intriguingly, foldamer **11** inhibited Aβ production 10-fold more potently than did **1**, though it retained inhibitory potency toward NICD. Although foldamer **1** showed preferential inhibition on NICD generation, simple incorporation of β^3-hSer at X_3 position increased inhibitory potency against Aβ without affecting NICD inhibition. This result indicates that β^3-hSer caused a substrate-specific effect

dx.doi.org/10.1021/jm301306c | J. Med. Chem. 2013, 56, 1443−1454

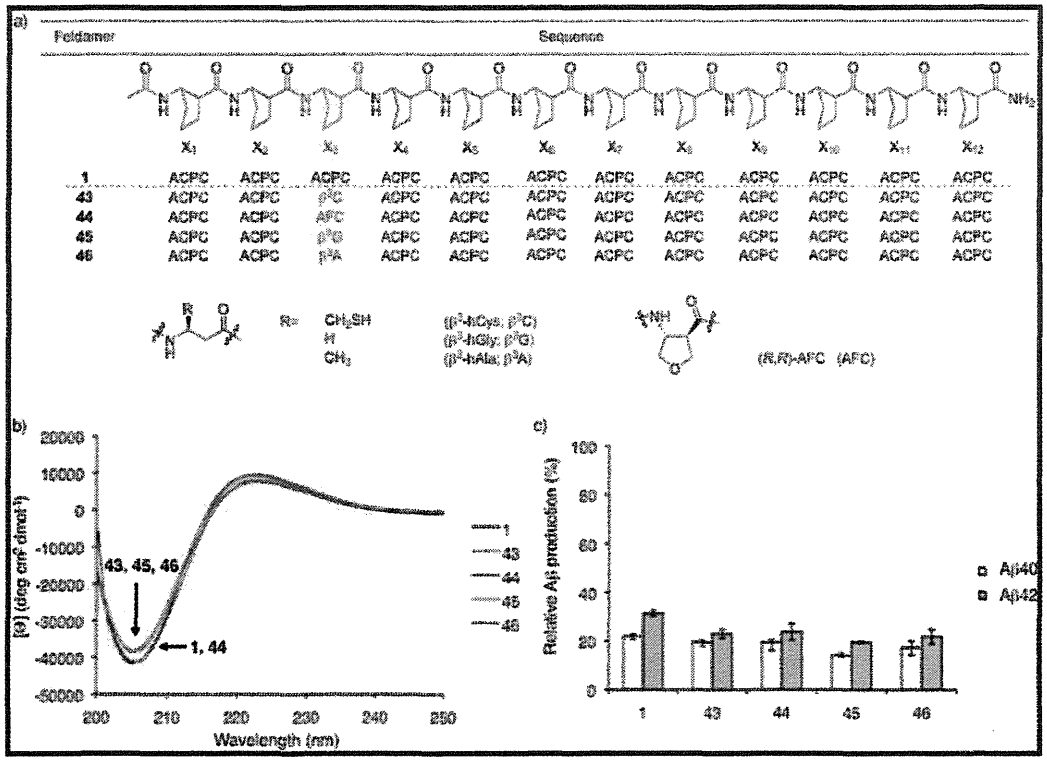

Figure 8. Structure, CD spectra, and γ-secretase-inhibitory activity of foldamers **43**–**46**. (a) Chemical structures. (b) CD spectra in methanol. The molar ellipticity [Θ] values have been normalized for oligomer concentration and the number of backbone amide groups. (c) Inhibition of γ-secretase activity by foldamers at 100 nM in an in vitro assay (n = 3).

Table 3. Inhibitory Potency of Foldamers toward γ-Secretase in in Vitro Assay (n = 3)

		IC_{50} (nM)	
compd	X_3	Aβ40	Aβ42
1	ACPC	8.81 ± 1.05	9.93 ± 2.14
11	β³-hSer	0.402 ± 0.0300	0.830 ± 0.111
12	β³-hAsn	0.555 ± 0.120	0.880 ± 0.0950
45	β³-hGly	2.47 ± 0.368	7.47 ± 2.04

Table 4. Inhibitory Potency of Foldamers in HEK293/NLNTK Cell Assay (n = 3)

		IC_{50} (μM)			
compd	X_3	IAβ40	Aβ42	NICD	NICD/Aβ42 IC_{50} ratio
1	ACPC	1.18	0.626	0.0204	0.0326
11	β³-hSer	0.0842	0.0864	0.0413	0.478
12	β³-hAsn	0.0846	0.0684	0.00316	0.0462

regarding γ-secretase inhibition. In contrast, **12** was 10-fold more potent than **1** for both Aβ and NICD generation. We also examined the effect of the foldamers on human H4 glioma cells, which express endogenous APP and Notch1 proteins (Figure 9). We did not observe any change in expression of either APP holoprotein or Notch1 in response to treatment with GSIs. In contrast, significant accumulation of APP CTF was detected, suggesting that foldamers inhibited the γ-secretase activity without affecting the expression of γ-substrates. Moreover, **11** and **12** showed more potent inhibitory activity than did **1**. Finally, to analyze the mode of inhibition by **11** and **12**, we

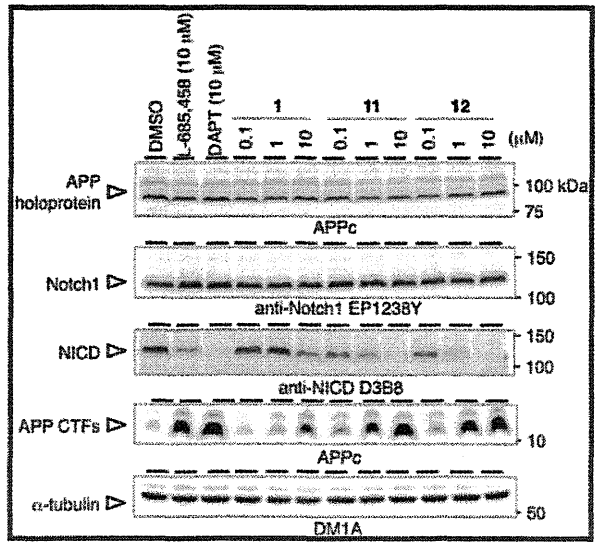

Figure 9. Effect of foldamers on the expression levels of endogenous γ-substrates in H4 glioma cells. Cells were treated with the indicated compounds for 24 h. Antibodies used for immunoblot analysis are shown under the panels.

examined these foldamers as competitors of the labeling of PS1 NTF by photoprobe **10** (Figure 10b). The biotinylation of PS1 NTF was almost completely blocked by preincubation with foldamers **11** and **12** in a similar fashion to that by foldamer **1**, suggesting that these foldamers share the same binding site.

dx.doi.org/10.1021/jm301306c | J. Med. Chem. 2013, 56, 1443–1454

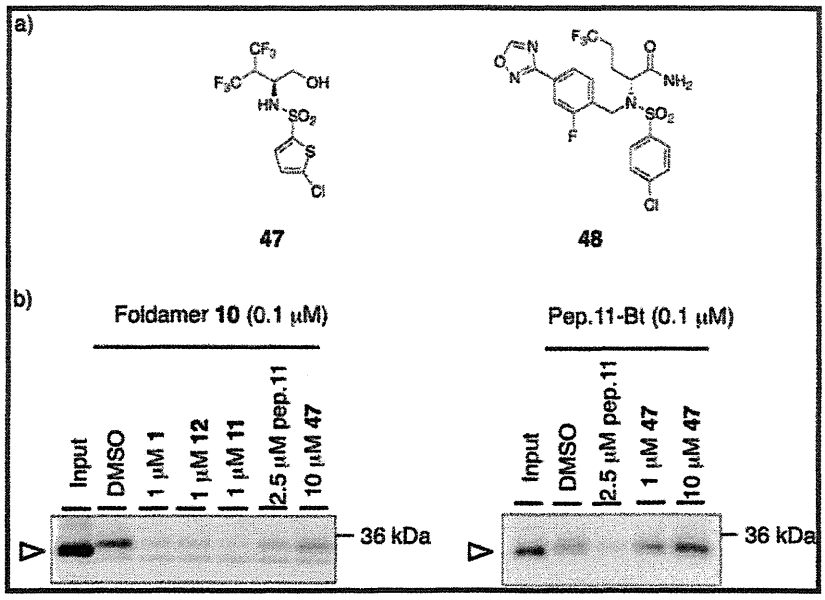

Figure 10. (a) Structures of sulfonamide-type Notch-sparing GSIs, begacestat **47**, and avagacestat **48**. (b) Cross-competition assay using **47** in a photoaffinity labeling experiment with **10** and pep.11-Bt.

These data support our in vitro finding that incorporation of β^3-hSer at the X_3 position of foldamers **1** provides increased substrate selectivity as well as increased inhibitory potency.

A series of sulfonamide/sulfone-containing small-molecular compounds have been identified as Notch-sparing GSIs.[6,7] These compounds predominantly inhibit Aβ production rather than Notch signaling in vivo, while they show similar potency against Aβ and NICD in in vitro γ-secretase assay.[52] Among Notch-sparing GSIs, begacestat **47** and avagacestat **48** have been tested in clinical trials.[6,7] However, the molecular mechanism whereby Notch-sparing GSIs show substrate selectivity remains unknown. To test whether the foldamer binding site in PS1 NTF is functionally correlated with the Notch-sparing effect of sulfonamide-type GSI, we tested the effect of begacestat (**47**) on photoaffinity labeling. Inhibitory activity of **47** was confirmed by in vitro γ-secretase assay (IC_{50} for Aβ40, 0.203 μM; IC_{50} for Aβ42, 0.414 μM). We found that the labeling of PS1 NTF by photoprobe **10** was significantly, but incompletely, reduced by preincubation with **47**, suggesting that the binding of Notch-sparing GSI allosterically affected the structure of the foldamer binding site (Figure 10). Surprisingly, however, **47** did not compete with the labeling of PS1 NTF by pep.11-Bt, a substrate-mimetic helical peptide-type GSI-based photoprobe. These data suggest that, in contrast to Aib-containing helical peptides, ACPC-based foldamers target not only the helix recognition region in the initial substrate docking site but also the domain involved in the mechanism of substrate selectivity.

As previously described, γ-secretase cleaves a wide variety of membrane proteins with no clear consensus sequence.[16] However, the results presented here indicate that the position and structure of side chain functional groups do in fact drastically affect the activity. Further studies to define the binding site of the photoprobe **10** in detail may provide insight into the molecular mechanism of the substrate selectivity of γ-secretase, as well as provide a basis for rational development of Notch-sparing small-molecular GSIs targeting the initial substrate docking site.

■ CONCLUSION

The results presented here and in our previous paper[12] clearly demonstrate the potential utility of 12-helical foldamers as GSIs. We have shown that compounds with the polyproline II helix lack γ-secretase-inhibitory activity, highlighting the importance of helix shape (i.e., the 12-helix) for the activity. As for length, ACPC 12mer seemed appropriate. The target site of foldamer **1** was directly identified as the initial substrate docking site by means of a photoaffinity labeling study, using photoprobe **10**. Further detailed examination of the binding site of photoprobe **10** is expected to provide protein-structural information about the initial substrate binding site in PS.

In order to improve the inhibitory potency and/or substrate selectivity of foldamer **1**, we prepared various derivatives by replacement of an ACPC residue with a linear β^3-amino acid. Various side chain functional groups were incorporated at diverse positions, and we identified foldamers **11** (X_3 = β^3-hSer) and **12** (X_3 = β^3-hAsn) as potent GSIs. Intriguingly, drastic position-specific effects were observed for incorporation of β^3-hSer, β^3-hAsn, β^3-hGlu, β^3-hLys, and β^3-hGln; i.e., substitution at the X_3 position is favorable for inhibitory activity, whereas the X_6 and X_9 positions are unfavorable. These results suggest that the foldamers are recognized at two binding sites of PS in position-specific manner. Notably, our cysteine-based structural analysis revealed that several TMDs of PS may have dual functions, dependent on topological location; the luminal side of TMD1, -6, and -9 is implicated in substrate binding via hydrophobic interaction.[53−55] In contrast, the cytosolic side of these TMDs directly faces the hydrophilic environment within the membrane. Thus, the $X_{6/9}$ positions in foldamers would bind with the luminal side of these TMDs. Moreover, small, neutral, and polar side chain groups at the X_3 position were found to be favorable for potent activity. In addition, a significant difference in inhibitory potencies toward

dx.doi.org/10.1021/jm301306c | J. Med. Chem. 2013, 56, 1443−1454

APP- and Notch-cleaving activities was observed between **11** and **12**, suggesting that the binding site of the X_3 residue in the foldamers is critical to the substrate selectivity of γ-secretase. In support of this notion, a known Notch-sparing GSI, begacestat, decreased the binding of the foldamer to PS1 NTF whereas it did not compete with the interaction between Aib-based helical peptide and PS1. Nevertheless, a more detailed analysis of the binding mode of these foldamers should be clarified further. Structural analysis of the γ-secretase using the foldamers may throw light on the molecular mechanism of substrate recognition.

In summary, our results demonstrate the potential value of foldamer-based inhibitors of γ-secretase. Through optimization, we have identified some of the substrate recognition properties of γ-secretase, which might offer clues for understanding the substrate selectivity and for developing Notch-sparing GSIs. The foldamer-based approach might be useful to explore substrate recognition of various intramembrane proteases.

EXPERIMENTAL SECTION

General. All reagents and solvents were of the highest commercial quality and were used without purification. Fmoc-*trans*-2-aminocyclopentanecarboxylic acid (Fmoc-ACPC-OH),[32] Fmoc-β[3]-amino acids,[44−48] were synthesized according to the cited references. Synthesis of Fmoc-(*R*,*R*)-AFC-OH is described in Supporting Information. Flash column chromatography was performed on silica gel (Fuji Silysia Chemical Ltd., BW-300) using forced flow. Thin layer chromatography (TLC) was performed on Merck precoated plates (silica gel 60 F254, 0.25 mm), and bands were visualized by fluorescence quenching under UV light or by staining with potassium permanganate or ninhydrin. ^{1}H NMR and ^{13}C NMR spectra were recorded on a JEOL LNM-LA500 at 500 and 125 MHz, respectively. Matrix-assisted laser desorption ionization-time-of-flight mass spectrometry (MALDI-TOF MS) was done with a Shimadzu AXIMA-CFR-NC using α-cyano-4-hydroxycinnamic acid as the matrix. Preparative RP-HPLC and analytical RP-HPLC were performed using a Shimadzu SPD-M10AVP variable-wavelength UV detector. Inertsil ODS-3 (10 mm × 250 mm, GL Science) and Inertsil ODS-3 (4.6 mm × 250 mm, GL Science) columns were employed for chromatographic and analytical separations, respectively. The purities of oligoproline peptides and β-peptide foldamers were >95%, as measured by comparing peak areas in analytical HPLC traces at 220 nm (see Supporting Information).

Synthesis of Oligoproline Peptides and β-Peptide Foldamers. Oligoproline peptides and β-peptides were synthesized with standard Fmoc solid-phase methods. Fmoc-NH-SAL-PEG resin (0.24 mmol/g, 100−200 mesh, 1% DVB) was employed for all peptide synthesis. For a typical 10 μmol scale synthesis, 42 mg of Fmoc-NH-SAL-PEG resin was swollen for 15 min in DMF.

Coupling Cycles. Amounts of 3 equiv of Fmoc-amino acid and 3 equiv of 2-(1*H*-benzotriazol-1-yl)-1,1,3,3-tetramethyluronium hexafluorophosphate (HBTU) and 3 equiv of 1-hydroxybenzotriazole monohydrate (HOBt·H_2O) were dissolved in 300 μL of DMF, and 6 equiv of *N*,*N*-diisopropylethylamine (DIEA) was added. The solution was added to resin bearing the N-deprotected peptide or β-peptide. The resin was agitated for 1−3 h.

Fmoc Deprotection Cycles. Fmoc deprotection was accomplished by adding to the resin 1.0 mL of 20% (v/v) piperidine in DMF and rocking for 30 min.

Acetylation. Acetylation of peptides was conducted for 2 h, by addition of 0.5 mL of 2:2:1 (v/v/v) Ac_2O/DMF/Et_3N to resin bearing the final desired N-deprotected peptide or β-peptide sequence.

Cleavage. Cleavage of all oligoproline peptides and β-peptides from the resin was accomplished by shaking the resin in a solution of trifluoroacetic acid (TFA)/triisopropylsilane (TIPS)/H_2O, 95:2.5:2.5 (0.5 mL), for 2 h. The resin was removed by filtration and rinsed with additional TFA. The combined filtrate was concentrated under a stream of Ar. Oligoproline peptides and β-peptides were precipitated from excess cold Et_2O and isolated by centrifugation. The crude oligoproline peptides and β-peptides thus obtained were purified by RP-HPLC.

CD Spectra. Dry peptide/foldamer samples were weighed on a microanalytical balance and dissolved in an appropriate amount of HPLC-grade methanol. Sample cells of 2 mm path length were used. Data were collected on a Jasco J-725 spectropolarimeter at 25 °C. Data were converted to mean residue ellipticity (deg cm^2 dmol^{-1}) according to the following equation:

$$[\Theta] = \frac{\psi M_r}{100lc}$$

where ψ is the CD signal in degrees, M_r is the molecular weight divided by the number of chromophores, l is the path length in decimeters, and c is the concentration in g/mL.

γ-Secretase Assay and Photoaffinity Labeling. γ-Secretase-inhibitory activity of oligoproline peptides and foldamers was measured using in vitro or cell-based assay as previously described.[12,31,51] H4 glioma cells were purchased from ATCC and maintained in DMEM with 10% FBS and Penicillin/Streptomycin. Photoaffinity labeling experiments using foldamer **10** as well as pep.11-Bt were performed as previously described.[12,14] *N*-[*N*-(3,5-Difluorophenacetyl)-L-alanyl]-(*S*)-phenylglycine *tert*-butyl ester (DAPT) was synthesized as previously reported.[56] Begacestat (**39**) was prepared according to the literature with slight modifications.[57,58] L-685,458 (Peptide Institute), pep.11 (BEX CO., LTD.), and pep.11-Bt (BEX CO., LTD.) were purchased from the indicated vendors. Anti-$PS1_{NT}$ and SPPCT for detection of PS1 NTF and SPP, respectively, were kindly provided by Drs. Gopal Thinakaran (The University of Chicago) and Todd Golde (University of Florida). Anti-nicastrin (N1660) (Sigma), anti-Aph-1aL (O2C2) (Covance), anti-APP C terminus (APPc) (Immuno-Biological Laboratories), anti-Notch C terminus (EP1238Y) (Epitomics), anti-NICD (D3B8) (Cell Signaling Technology), and anti-α-tubulin (DM1A) (Sigma) antibodies were purchased from the indicated vendors. anti-Pen-2 PNT3 was reported previously.[59]

ASSOCIATED CONTENT

Supporting Information

Synthesis of Fmoc-(R,R)-AFC-OH, identification of oligoproline peptides and foldamers, CD spectra and γ-secretase-inhibitory activity of photoprobe **10**, *and chemical structure of pep.11-Bt. This material is available free of charge via the Internet at http://pubs.acs.org.*

AUTHOR INFORMATION

Corresponding Author

*For N.U.: phone, +81-52-836-3438; e-mail, umezawa@phar.nagoya-cu.ac.jp. For T.T.: phone, +81-3-5841-4868; e-mail, taisuke@mol.f.u-tokyo.ac.jp. For T.H.: phone, +81-52-836-3435; e-mail, higuchi@phar.nagoya-cu.ac.jp.

Notes

The authors declare no competing financial interest.

ACKNOWLEDGMENTS

This work was supported in part by Grants-in-Aid for Scientific Research (A) (T.H.), (C) (N.U.), Grants-in-Aid for Young Scientists (S) (T.T.) from the Japan Society for the Promotion of Science (JSPS), and grants from the Targeted Proteins Research Program of the Japan Science and Technology Agency (JST) (T.I., T.T.), and Takeda Memorial Foundation (N.U.). Y.I. is a research fellow of JSPS.

REFERENCES

(1) Holtzman, D. M.; Morris, J. C.; Goate, A. M. Alzheimer's disease: the challenge of the second century. *Sci. Transl. Med.* **2011**, 3, 77sr1.

(2) Iwatsubo, T.; Odaka, A.; Suzuki, N.; Mizusawa, H.; Nukina, N.; Ihara, Y. Visualization of Aβ42(43) and Aβ40 in senile plaques with end-specific Aβ monoclonals: evidence that an initially deposited species is Aβ42(43). *Neuron* **1994**, *13*, 45−53.
(3) Tomita, T. Secretase inhibitors and modulators for Alzheimer's disease treatment. *Expert Rev. Neurother.* **2009**, *9*, 661−679.
(4) De Strooper, B.; Vassar, R.; Golde, T. The secretases: enzymes with therapeutic potential in Alzheimer disease. *Nat. Rev. Neurol.* **2010**, *6*, 99−107.
(5) Wolfe, M. S. γ-Secretase inhibitors and modulators for Alzheimer's disease. *J. Neurochem.* **2012**, *120* (Suppl. 1), 89−98.
(6) Kreft, A. F.; Martone, R.; Porte, A. Recent advances in the identification of γ-secretase inhibitors to clinically test the Aβ oligomer hypothesis of Alzheimer's disease. *J. Med. Chem.* **2009**, *52*, 6169−6188.
(7) Oehlrich, D.; Berthelot, D. J.-C.; Gijsen, H. J. M. γ-Secretase modulators as potential disease modifying anti-Alzheimer's drugs. *J. Med. Chem.* **2011**, *54*, 669−698.
(8) Takasugi, N.; Tomita, T.; Hayashi, I.; Tsuruoka, M.; Niimura, M.; Takahashi, Y.; Thinakaran, G.; Iwatsubo, T. The role of presenilin cofactors in the γ-secretase complex. *Nature* **2003**, *422*, 438−441.
(9) Li, Y. M.; Xu, M.; Lai, M. T.; Huang, Q.; Castro, J. L.; DiMuzio-Mower, J.; Harrison, T.; Lellis, C.; Nadin, A.; Neduvelil, J. G.; Register, R. B.; Sardana, M. K.; Shearman, M. S.; Smith, A. L.; Shi, X. P.; Yin, K. C.; Shafer, J. A.; Gardell, S. J. Photoactivated γ-secretase inhibitors directed to the active site covalently label presenilin 1. *Nature* **2000**, *405*, 689−694.
(10) Xu, M.; Lai, M.-T.; Huang, Q.; DiMuzio-Mower, J.; Castro, J. L.; Harrison, T.; Nadin, A.; Neduvelil, J. G.; Shearman, M. S.; Shafer, J. A.; Gardell, S. J.; Li, Y.-M. γ-Secretase: characterization and implication for Alzheimer disease therapy. *Neurobiol. Aging* **2002**, *23*, 1023−1030.
(11) Kornilova, A. Y.; Bihel, F.; Das, C.; Wolfe, M. S. The initial substrate-binding site of γ-secretase is located on presenilin near the active site. *Proc. Natl. Acad. Sci. U.S.A.* **2005**, *102*, 3230−3235.
(12) Imamura, Y.; Watanabe, N.; Umezawa, N.; Iwatsubo, T.; Kato, N.; Tomita, T.; Higuchi, T. Inhibition of γ-secretase activity by helical β-peptide foldamers. *J. Am. Chem. Soc.* **2009**, *131*, 7353−7359.
(13) Fuwa, H.; Takahashi, Y.; Konno, Y.; Watanabe, N.; Miyashita, H.; Sasaki, M.; Natsugari, H.; Kan, T.; Fukuyama, T.; Tomita, T.; Iwatsubo, T. Divergent synthesis of multifunctional molecular probes to elucidate the enzyme specificity of dipeptidic γ-secretase inhibitors. *ACS Chem. Biol.* **2007**, *2*, 408−418.
(14) Morohashi, Y.; Kan, T.; Tominari, Y.; Fuwa, H.; Okamura, Y.; Watanabe, N.; Sato, C.; Natsugari, H.; Fukuyama, T.; Iwatsubo, T.; Tomita, T. C-terminal fragment of presenilin is the molecular target of a dipeptidic γ-secretase-specific inhibitor DAPT (*N*-[*N*-(3,5-difluorophenacetyl)-L-alanyl]-*S*-phenylglycine *t*-butyl ester. *J. Biol. Chem.* **2006**, *281*, 14670−14676.
(15) Haapasalo, A.; Kovacs, D. M. The many substrates of presenilin/γ-secretase. *J. Alzheimer's Dis.* **2011**, *25*, 3−28.
(16) Beel, A. J.; Sanders, C. R. Substrate specificity of γ-secretase and other intramembrane proteases. *Cell. Mol. Life Sci.* **2008**, *65*, 1311−1334.
(17) Searfoss, G. H.; Jordan, W. H.; Calligaro, D. O.; Galbreath, E. J.; Schirtzinger, L. M.; Berridge, B. R.; Gao, H.; Higgins, M. A.; May, P. C.; Ryan, T. P. Adipsin, a biomarker of gastrointestinal toxicity mediated by a functional γ-secretase inhibitor. *J. Biol. Chem.* **2003**, *278*, 46107−46116.
(18) Wong, G. T.; Manfra, D.; Poulet, F. M.; Zhang, Q.; Josien, H.; Bara, T.; Engstrom, L.; Pinzon-Ortiz, M.; Fine, J. S.; Lee, H.-J. J.; Zhang, L.; Higgins, G. A.; Parker, E. M. Chronic treatment with the γ-secretase inhibitor LY-411,575 inhibits β-amyloid peptide production and alters lymphopoiesis and intestinal cell differentiation. *J. Biol. Chem.* **2004**, *279*, 12876−12882.
(19) Gellman, S. H. Foldamers: a manifesto. *Acc. Chem. Res.* **1998**, *31*, 173−180.
(20) Seebach, D.; Beck, A. K.; Bierbaum, D. J. The world of β- and γ-peptides comprised of homologated proteinogenic amino acids and other components. *Chem. Biodiversity* **2004**, *1*, 1111−1239.
(21) Cheng, R. P.; Gellman, S. H.; DeGrado, W. F. β-Peptides: from structure to function. *Chem. Rev.* **2001**, *101*, 3219−3232.
(22) Das, C.; Berezovska, O.; Diehl, T. S.; Genet, C.; Buldyrev, I.; Tsai, J.-Y.; Hyman, B. T.; Wolfe, M. S. Designed helical peptides inhibit an intramembrane protease. *J. Am. Chem. Soc.* **2003**, *125*, 11794−11795.
(23) Bihel, F.; Das, C.; Bowman, M. J.; Wolfe, M. S. Discovery of a subnanomolar helical D-tridecapeptide inhibitor of γ-secretase. *J. Med. Chem.* **2004**, *47*, 3931−3933.
(24) Karle, I. L.; Balaram, P. Structural characteristics of α-helical peptide molecules containing Aib residues. *Biochemistry* **1990**, *29*, 6747−6756.
(25) Balaram, P. Non-standard amino acids in peptide design and protein engineering. *Curr. Opin. Struct. Biol.* **1992**, *2*, 845−851.
(26) Porter, E. A.; Weisblum, B.; Gellman, S. H. Mimicry of host-defense peptides by unnatural oligomers: antimicrobial β-peptides. *J. Am. Chem. Soc.* **2002**, *124*, 7324−7330.
(27) Crisma, M.; Formaggio, F.; Moretto, A.; Toniolo, C. Peptide helices based on α-amino acids. *Biopolymers* **2006**, *84*, 3−12.
(28) Barlow, D. J.; Thornton, J. M. Helix geometry in proteins. *J. Mol. Biol.* **1988**, *201*, 601−619.
(29) Choi, S. H.; Guzei, I. a; Spencer, L. C.; Gellman, S. H. Crystallographic characterization of 12-helical secondary structure in β-peptides containing side chain groups. *J. Am. Chem. Soc.* **2010**, *132*, 13879−13885.
(30) Rabanal, F.; Ludevid, M. D.; Pons, M.; Giralt, E. CD of proline-rich polypeptides: application to the study of the repetitive domain of maize glutelin-2. *Biopolymers* **1993**, *33*, 1019−1028.
(31) Takahashi, Y.; Hayashi, I.; Tominari, Y.; Rikimaru, K.; Morohashi, Y.; Kan, T.; Natsugari, H.; Fukuyama, T.; Tomita, T.; Iwatsubo, T. Sulindac sulfide is a noncompetitive γ-secretase inhibitor that preferentially reduces Aβ42 generation. *J. Biol. Chem.* **2003**, *278*, 18664−18670.
(32) LePlae, P. R.; Umezawa, N.; Lee, H. S.; Gellman, S. H. An efficient route to either enantiomer of *trans*-2-aminocyclopentanecarboxylic acid. *J. Org. Chem.* **2001**, *66*, 5629−5632.
(33) Appella, D. H.; Christianson, L. A.; Klein, D. A.; Powell, D. R.; Huang, X.; Barchi, J. J.; Gellman, S. H. Residue-based control of helix shape in β-peptide oligomers. *Nature* **1997**, *387*, 381−384.
(34) Applequist, J.; Bode, K. A.; Appella, D. H.; Christianson, L. A.; Gellman, S. H. Theoretical and experimental circular dichroic spectra of the novel helical foldamer poly[(1*R*,2*R*)-*trans*-2-aminocyclopentanecarboxylic acid]. *J. Am. Chem. Soc.* **1998**, *120*, 4891−4892.
(35) Appella, D. H.; Christianson, L. A.; Klein, D. A.; Richards, M. R.; Powell, D. R.; Gellman, S. H. Synthesis and structural characterization of helix-forming β-peptides: *trans*-2-aminocyclopentanecarboxylic acid oligomers. *J. Am. Chem. Soc.* **1999**, *121*, 7574−7581.
(36) Dorman, G.; Prestwich, G. D. Benzophenone photophores in biochemistry. *Biochemistry* **1994**, *33*, 5661−5673.
(37) Fluhrer, R.; Haass, C. Signal peptide peptidases and γ-secretase: cousins of the same protease family? *Neurodegener. Dis.* **2007**, *4*, 112−116.
(38) Nyborg, A. C.; Jansen, K.; Ladd, T. B.; Fauq, A.; Golde, T. E. A signal peptide peptidase (SPP) reporter activity assay based on the cleavage of type II membrane protein substrates provides further evidence for an inverted orientation of the SPP active site relative to presenilin. *J. Biol. Chem.* **2004**, *279*, 43148−43156.
(39) Weihofen, A.; Lemberg, M. K.; Friedmann, E.; Rueeger, H.; Schmitz, A.; Paganetti, P.; Rovelli, G.; Martoglio, B. Targeting presenilin-type aspartic protease signal peptide peptidase with γ-secretase inhibitors. *J. Biol. Chem.* **2003**, *278*, 16528−16533.
(40) Sato, T.; Nyborg, A. C.; Iwata, N.; Diehl, T. S.; Saido, T. C.; Golde, T. E.; Wolfe, M. S. Signal peptide peptidase: biochemical properties and modulation by nonsteroidal antiinflammatory drugs. *Biochemistry* **2006**, *45*, 8649−8656.
(41) Sato, T.; Ananda, K.; Cheng, C. I.; Suh, E. J.; Narayanan, S.; Wolfe, M. S. Distinct pharmacological effects of inhibitors of signal peptide peptidase and γ-secretase. *J. Biol. Chem.* **2008**, *283*, 33287−33295.

(42) Frackenpohl, J.; Arvidsson, P. I.; Schreiber, J. V.; Seebach, D. The outstanding biological stability of β- and γ-peptides toward proteolytic enzymes: an in vitro investigation with fifteen peptidases. *ChemBioChem* **2001**, *2*, 445–455.
(43) LePlae, P. R.; Fisk, J. D.; Porter, E. A.; Weisblum, B.; Gellman, S. H. Tolerance of acyclic residues in the β-peptide 12-helix: access to diverse side-chain arrays for biological applications. *J. Am. Chem. Soc.* **2002**, *124*, 6820–6821.
(44) Guichard, G.; Abele, S.; Seebach, D. Preparation of *N*-Fmoc-protected β^2- and β^3-amino acids and their use as building blocks for the solid-phase synthesis of β-peptides. *Helv. Chim. Acta* **1998**, *81*, 187–206.
(45) Müller, A.; Vogt, C.; Sewald, N. Synthesis of Fmoc-β-homoamino acids by ultrasound-promoted Wolff rearrangement. *Synthesis* **1998**, 837–841.
(46) Gademann, K.; Kimmerlin, T.; Hoyer, D.; Seebach, D. Peptide folding induces high and selective affinity of a linear and small β-peptide to the human somatostatin receptor 4. *J. Med. Chem.* **2001**, *44*, 2460–2468.
(47) Lelais, G.; Micuch, P.; Josien-Lefebvre, D.; Rossi, F.; Seebach, D. Preparation of protected β^2- and β^3-homocysteine, β^2- and β^3-homohistidine, and β^2-homoserine for solid-phase syntheses. *Helv. Chim. Acta* **2004**, *87*, 3131–3159.
(48) Wilczyńska, D.; Kosson, P.; Kwasiborska, M.; Ejchart, A.; Olma, A. Synthesis and receptor binding of opioid peptide analogues containing β^3-homo-amino acids. *J. Pept. Sci.* **2009**, *15*, 777–782.
(49) Bunnage, M. E.; Davies, S. G.; Roberts, P. M.; Smith, A. D.; Withey, J. M. Asymmetric synthesis of the *cis*- and *trans*-stereoisomers of 4-aminopyrrolidine-3-carboxylic acid and 4-aminotetrahydrofuran-3-carboxylic acid. *Org. Biomol. Chem.* **2004**, *2*, 2763–2776.
(50) Liu, W.; Crocker, E.; Zhang, W.; Elliott, J. I.; Luy, B.; Li, H.; Aimoto, S.; Smith, S. O. Structural role of glycine in amyloid fibrils formed from transmembrane α-helices. *Biochemistry* **2005**, *44*, 3591–3597.
(51) Ohki, Y.; Higo, T.; Uemura, K.; Shimada, N.; Osawa, S.; Berezovska, O.; Yokoshima, S.; Fukuyama, T.; Tomita, T.; Iwatsubo, T. Phenylpiperidine-type γ-secretase modulators target the transmembrane domain 1 of presenilin 1. *EMBO J.* **2011**, *30*, 4815–4824.
(52) Chávez-Gutiérrez, L.; Bammens, L.; Benilova, I.; Vandersteen, A.; Benurwar, M.; Borgers, M.; Lismont, S.; Zhou, L.; Cleynenbreugel, S.; Van; Esselmann, H.; Wiltfang, J.; Serneels, L.; Karran, E.; Gijsen, H.; Schymkowitz, J.; Rousseau, F.; Broersen, K.; De Strooper, B. The mechanism of γ-secretase dysfunction in familial Alzheimer disease. *EMBO J.* **2012**, *31*, 2261–2274.
(53) Sato, C.; Takagi, S.; Tomita, T.; Iwatsubo, T. The C-terminal PAL motif and transmembrane domain 9 of presenilin 1 are involved in the formation of the catalytic pore of the γ-secretase. *J. Neurosci.* **2008**, *28*, 6264–6271.
(54) Watanabe, N.; Image Image, I. I.; Takagi, S.; Tominaga, A.; Image Image, I.; Tomita, T.; Iwatsubo, T. Functional analysis of the transmembrane domains of presenilin 1: participation of transmembrane domains 2 and 6 in the formation of initial substrate-binding site of γ-secretase. *J. Biol. Chem.* **2010**, *285*, 19738–19746.
(55) Takagi, S.; Tominaga, A.; Sato, C.; Tomita, T.; Iwatsubo, T. Participation of transmembrane domain 1 of presenilin 1 in the catalytic pore structure of the γ-secretase. *J. Neurosci.* **2010**, *30*, 15943–15950.
(56) Kan, T.; Tominari, Y.; Rikimaru, K.; Morohashi, Y.; Natsugari, H.; Tomita, T.; Iwatsubo, T.; Fukuyama, T. Parallel synthesis of DAPT derivatives and their γ-secretase-inhibitory activity. *Bioorg. Med. Chem. Lett.* **2004**, *14*, 1983–1985.
(57) Mayer, S. C.; Kreft, A. F.; Harrison, B.; Abou-Gharbia, M.; Antane, M.; Aschmies, S.; Atchison, K.; Chlenov, M.; Cole, D. C.; Comery, T.; Diamantidis, G.; Ellingboe, J.; Fan, K.; Galante, R.; Gonzales, C.; Ho, D. M.; Hoke, M. E.; Hu, Y.; Huryn, D.; Jain, U.; Jin, M.; Kremer, K.; Kubrak, D.; Lin, M.; Lu, P.; Magolda, R.; Martone, R.; Moore, W.; Oganesian, A.; Pangalos, M. N.; Porte, A.; Reinhart, P.; Resnick, L.; Riddell, D. R.; Sonnenberg-Reines, J.; Stock, J. R.; Sun, S.-C.; Wagner, E.; Wang, T.; Woller, K.; Xu, Z.; Zaleska, M. M.; Zeldis, J.; Zhang, M.; Zhou, H.; Jacobsen, J. S. Discovery of begacestat, a Notch-1-sparing γ-secretase inhibitor for the treatment of Alzheimer's disease. *J. Med. Chem.* **2008**, *51*, 7348–7351.
(58) Keese, R.; Hinderling, C. Efficient synthesis of (*S*)-methyl hexafluorovalinate. *Synthesis* **1996**, 695–696.
(59) Isoo, N.; Sato, C.; Miyashita, H.; Shinohara, M.; Takasugi, N.; Morohashi, Y.; Tsuji, S.; Tomita, T.; Iwatsubo, T. Aβ42 overproduction associated with structural changes in the catalytic pore of γ-secretase: common effects of Pen-2 N-terminal elongation and fenofibrate. *J. Biol. Chem.* **2007**, *282*, 12388–12396.

Science Translational Medicine
AAAS

Drug Screening for ALS Using Patient-Specific Induced Pluripotent Stem Cells

Naohiro Egawa *et al.*

Sci Transl Med **4**, 145ra104 (2012);
DOI: 10.1126/scitranslmed.3004052

Editor's Summary

A Stepping Stone to ALS Drug Screening

Amyotrophic lateral sclerosis (ALS) is an untreatable disorder in which the motor neurons degenerate, resulting in paralysis and death. Induced pluripotent stem cell (iPSC) technology makes it possible to analyze motor neurons from patients with ALS and to use them for screening new candidate drugs. In new work, Egawa *et al.* obtained motor neurons by inducing differentiation of iPSC lines derived from several patients with familial ALS. These patients carried disease-causing mutations in the gene encoding Tar DNA binding protein-43 (TDP-43). The ALS motor neurons in culture recapitulated cellular and molecular abnormalities associated with ALS. For example, the authors found that mutant TDP-43 in the ALS motor neurons perturbed RNA metabolism and that the motor neurons were more vulnerable to cellular stressors such as arsenite. The researchers then used the ALS motor neurons in a drug screening assay and identified a compound called anacardic acid, a histone acetyltransferase inhibitor, that could reverse some of the ALS phenotypes observed in the motor neurons. The new work provides an encouraging step toward using motor neurons generated from iPSCs derived from ALS patients to learn more about what triggers the death of motor neurons in this disease and to identify new candidate drugs that may be able to slow or reverse the devastating loss of motor neurons.

Science Translational Medicine (print ISSN 1946-6234; online ISSN 1946-6242) is published weekly, except the last week in December, by the American Association for the Advancement of Science, 1200 New York Avenue NW, Washington, DC 20005.

STEM CELLS

Drug Screening for ALS Using Patient-Specific Induced Pluripotent Stem Cells

Naohiro Egawa,[1,2]* Shiho Kitaoka,[1,2]* Kayoko Tsukita,[1,2] Motoko Naitoh,[3] Kazutoshi Takahashi,[1] Takuya Yamamoto,[1,4] Fumihiko Adachi,[1] Takayuki Kondo,[1,5] Keisuke Okita,[1] Isao Asaka,[1] Takashi Aoi,[1] Akira Watanabe,[1,4] Yasuhiro Yamada,[1,4] Asuka Morizane,[1,6] Jun Takahashi,[1,6] Takashi Ayaki,[5] Hidefumi Ito,[5] Katsuhiro Yoshikawa,[3] Satoko Yamawaki,[3] Shigehiko Suzuki,[3] Dai Watanabe,[7] Hiroyuki Hioki,[8] Takeshi Kaneko,[8] Kouki Makioka,[9] Koichi Okamoto,[9] Hiroshi Takuma,[10] Akira Tamaoka,[10] Kazuko Hasegawa,[11] Takashi Nonaka,[12] Masato Hasegawa,[12] Akihiro Kawata,[13] Minoru Yoshida,[14] Tatsutoshi Nakahata,[1] Ryosuke Takahashi,[5] Maria C. N. Marchetto,[15] Fred H. Gage,[15] Shinya Yamanaka,[1,4,16] Haruhisa Inoue[1,2,16†]

Amyotrophic lateral sclerosis (ALS) is a late-onset, fatal disorder in which the motor neurons degenerate. The discovery of new drugs for treating ALS has been hampered by a lack of access to motor neurons from ALS patients and appropriate disease models. We generate motor neurons from induced pluripotent stem cells (iPSCs) from familial ALS patients, who carry mutations in Tar DNA binding protein-43 (TDP-43). ALS patient–specific iPSC–derived motor neurons formed cytosolic aggregates similar to those seen in postmortem tissue from ALS patients and exhibited shorter neurites as seen in a zebrafish model of ALS. The ALS motor neurons were characterized by increased mutant TDP-43 protein in a detergent-insoluble form bound to a spliceosomal factor SNRPB2. Expression array analyses detected small increases in the expression of genes involved in RNA metabolism and decreases in the expression of genes encoding cytoskeletal proteins. We examined four chemical compounds and found that a histone acetyltransferase inhibitor called anacardic acid rescued the abnormal ALS motor neuron phenotype. These findings suggest that motor neurons generated from ALS patient–derived iPSCs may provide a useful tool for elucidating ALS disease pathogenesis and for screening drug candidates.

INTRODUCTION

Amyotrophic lateral sclerosis (ALS) is a neurodegenerative disorder characterized by a loss of upper and lower motor neurons that typically develops in the fifth or sixth decade of life, with a survival of less than 5 years and a prevalence of 2 in 100,000 (*1*, *2*). The histopathological hallmarks of this fatal disease include cytosolic aggregates in the motor neurons of most ALS patients with the sporadic form of the disease. These aggregates are composed of Tar DNA binding protein-43 (TDP-43) (*3*–*5*), a 414–amino acid nuclear mRNA binding protein containing two RNA recognition motifs. Genetic analysis has identified more than 30 mutations in the *TDP-43* gene in both familial and sporadic ALS cases (*6*). ALS-associated abnormalities have been reported in patient samples and cellular and animal models (*6*–*10*), and several compounds have been identified as abrogating the disease phenotype in an ALS mouse model. However, when these compounds were tested in ALS patients, no clinical improvements were observed (*11*).

Induced pluripotent stem cells (iPSCs) have been generated from ALS patients and differentiated into motor neurons (*12*, *13*), but it is not yet clear whether the abnormal cellular and molecular phenotypes of ALS can be recapitulated in vitro. A lack of access to human motor neurons and appropriate disease models has hampered efforts to test new drug candidates for ALS. Here, we generated human motor neurons from iPSCs derived from familial ALS patients carrying *TDP-43* mutations and used them to identify a compound that rescued the ALS-associated phenotype.

RESULTS

Spinal motor neurons were generated from iPSCs derived from dermal fibroblasts from patients with familial ALS or from control individuals by means of retroviral or episomal vectors. Seven control human iPSC lines were derived from five unrelated individuals without mutations in the *TDP-43* gene, and nine ALS iPSC lines were generated from three ALS patients with mutations in *TDP-43* (*14*, *15*) (Fig. 1A, fig. S1A, and table S1). ALS patients A21, A34, and ND32947 were heterozygous for the Q343R, M337V, and G298S mutations in *TDP-43*, respectively. Neural populations including motor neurons derived from the ALS patient iPSCs retained these *TDP-43* mutations (Fig. 1B).

[1]Center for iPS Cell Research and Application (CiRA), Kyoto University, Kyoto 606-8507, Japan. [2]Core Research for Evolutional Science and Technology (CREST), Japan Science and Technology Agency, Tokyo 102-0076, Japan. [3]Department of Plastic and Reconstructive Surgery, Graduate School of Medicine, Kyoto University, Kyoto 606-8507, Japan. [4]Institute for Integrated Cell-Material Sciences, Kyoto University, Kyoto 606-8501, Japan. [5]Department of Neurology, Graduate School of Medicine, Kyoto University, Kyoto 606-8507, Japan. [6]Department of Biological Repair, Institute for Frontier Medical Sciences, Kyoto University, Kyoto 606-8507, Japan. [7]Department of Biological Sciences, Graduate School of Medicine and Department of Molecular and Systems Biology, Graduate School of Biostudies, Kyoto University, Kyoto 606-8501, Japan. [8]Department of Morphological Brain Science, Graduate School of Medicine, Kyoto University, Kyoto 606-8501, Japan. [9]Department of Neurology, Gunma University Graduate School of Medicine, Maebashi 371-8511, Japan. [10]Department of Neurology, Institute of Clinical Medicine, University of Tsukuba, Tsukuba 305-8576, Japan. [11]Department of Neurology, Sagamihara Hospital, Sagamihara 252-0392, Japan. [12]Department of Neuropathology and Cell Biology, Tokyo Metropolitan Institute of Medical Science, Tokyo 156-8506, Japan. [13]Department of Neurology, Tokyo Metropolitan Neurological Hospital, Tokyo 183-0042, Japan. [14]Chemical Genetics Laboratory Molecular Ligand Biology Research Team, Chemical Genomics Research Group, RIKEN Advanced Science Institute, Wako, Saitama 351-0198, Japan. [15]The Salk Institute for Biological Studies, La Jolla, CA 92037, USA. [16]Yamanaka iPS Cell Special Project, Japan Science and Technology Agency, Kawaguchi 332-0012, Japan.
*These authors contributed equally to this work.
†To whom correspondence should be addressed. E-mail: haruhisa@cira.kyoto-u.ac.jp

The iPSCs generated from ALS and control dermal fibroblasts expressed human embryonic stem cell (ESC) markers (Fig. 1A and fig. S1A) and were fully characterized (figs. S1 to S5 and table S2). The ALS and control iPSC lines were then differentiated into motor neurons (*16*) (Fig. 1C and fig. S6A). Differentiated motor neurons were identified by expression of motor neuron markers including Islet-1, HB9, SMI-32, and ChAT (choline acetyltransferase) (Fig. 1C and fig. S6B), and their function was verified by coculture with myotubes (fig. S6, D to F). To visualize live motor neurons, we transduced them with lentivirus expressing green fluorescent protein (GFP) under the control of the HB9 promoter (HB9::GFP) (*17*) (Fig. 1C). HB9::GFP-positive neurons colocalized with ChAT (fig. S6C) and showed spontaneous action potentials and synaptic potentials (fig. S6, G to K). Immunocytochemical analysis with MAP2, SMI-32, and GFAP (glial fibrillary acidic protein) did not reveal any differences in differentiation propensity between ALS and control iPSCs (Fig. 1, D to G, and fig. S7).

Next, we examined whether ALS iPSC-derived motor neurons have shorter neurites as reported in an ALS zebrafish model (*6*) and decreased neurofilament mRNA as reported in postmortem tissues from ALS patients (*7*, *18*). ALS iPSC-derived motor neurons expressing HB9::GFP were purified by fluorescence-activated cell sorting (FACS) (*17*, *19*) (Fig. 2A and fig. S8, A to C). ALS iPSC-derived motor neurons showed shorter neurites [33.5 ± 9.9 μm (mean ± SD) compared to 63.8 ± 13.1 μm for control; $P = 2.0 \times 10^{-4}$ by *t* test] (Fig. 2, A and B, and fig. S9A). Gene expression profiling of the purified ALS iPSC-derived motor neurons showed that there was a decrease in expression of genes encoding components of cytoskeletal intermediate filaments (control > ALS, fold change >1.2, $P < 0.01$) (Fig. 2D, fig. S8, F and G, and table S4). The expression of medium polypeptide neurofilament (NEFM) and light polypeptide neurofilament (NEFL) was significantly decreased in ALS compared to control iPSC-derived motor neurons [$P = 7.9 \times 10^{-3}$ (NEFL); $P = 5.3 \times 10^{-3}$ (NEFM); *t* test] (Fig. 2C and table S6).

TDP-43 is involved in multiple steps of RNA metabolism, including transcription, splicing, and transport of mRNA (*20*–*22*). TDP-43 protein autoregulates its synthesis by binding to the 3′ untranslated region of its own mRNA in a negative feedback loop (*8*). Gene expression profiles of purified ALS iPSC-derived motor neurons demonstrated that gene ontology (GO) terms related to RNA binding, splicing, processing, and transcriptional initiation were enriched compared to the profiles of control iPSC-derived motor neurons (Fig. 2D). The transcripts of nuclear transport/RNA granule and spliceosomal complex–related genes were also up-regulated in ALS iPSC-derived motor neurons (Fig. 2D, fig. S8, D, E, and G, and tables S3 and S5), indicating that RNA metabolism may be perturbed in ALS compared to control iPSC-derived motor

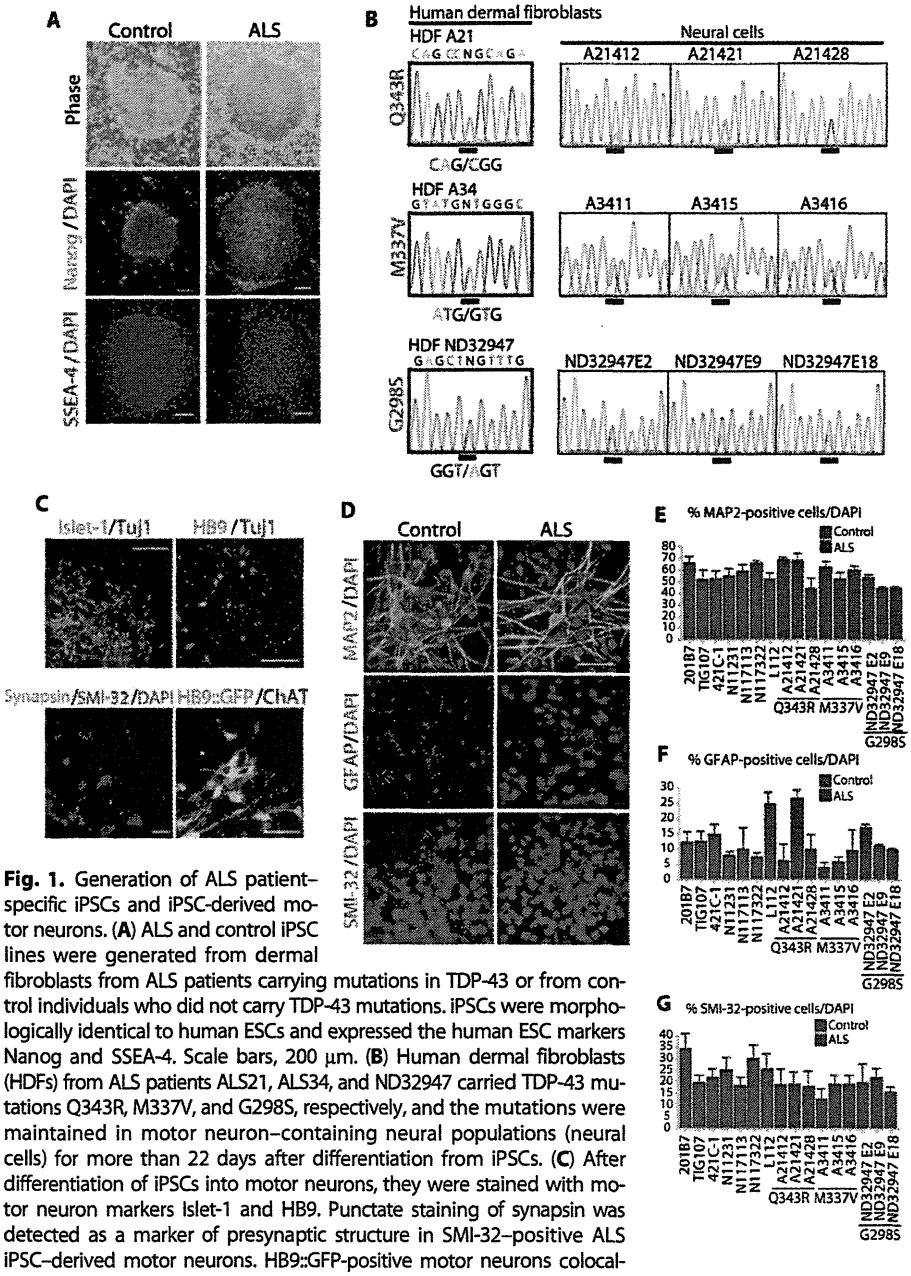

Fig. 1. Generation of ALS patient-specific iPSCs and iPSC-derived motor neurons. (**A**) ALS and control iPSC lines were generated from dermal fibroblasts from ALS patients carrying mutations in TDP-43 or from control individuals who did not carry TDP-43 mutations. iPSCs were morphologically identical to human ESCs and expressed the human ESC markers Nanog and SSEA-4. Scale bars, 200 μm. (**B**) Human dermal fibroblasts (HDFs) from ALS patients ALS21, ALS34, and ND32947 carried TDP-43 mutations Q343R, M337V, and G298S, respectively, and the mutations were maintained in motor neuron–containing neural populations (neural cells) for more than 22 days after differentiation from iPSCs. (**C**) After differentiation of iPSCs into motor neurons, they were stained with motor neuron markers Islet-1 and HB9. Punctate staining of synapsin was detected as a marker of presynaptic structure in SMI-32–positive ALS iPSC-derived motor neurons. HB9::GFP-positive motor neurons colocalized with ChAT. Scale bars, 50 μm. (**D** to **G**) Motor neuron differentiation from ALS and control iPSCs. After 2 months of differentiation from iPSCs in culture, motor neurons were stained with the MAP2 neuronal marker and the motor neuron–specific marker SMI-32. Astrocytes were revealed by staining with GFAP. Scale bar, 50 μm. Proportions of ALS and control iPSC-derived motor neurons staining positive for MAP2 (E), GFAP (F), and SMI-32 (G) are shown. Error bars are SD.

neurons (*8*, *20*). The expression of TDP-43 mRNA was significantly increased in ALS iPSC–derived motor neurons compared to control ($P = 0.040$ by t test; Fig. 2E and fig. S8, D and G) (*8*, *23*).

TDP-43 has been reported in the detergent-insoluble fraction of postmortem tissues from ALS patients (*3*, *4*, *24*) and has been shown to be mislocalized, forming cytoplasmic preinclusions (*20*). To analyze the biochemical properties of TDP-43 in ALS iPSC–derived neural populations containing motor neurons, we performed Western blot analysis. The amount of detergent-insoluble TDP-43 including full-length and smaller fragments increased markedly in ALS iPSC–derived motor neuron–containing neural populations (Fig. 2F and fig. S9B). Immunocytochemical analysis revealed that TDP-43 in control

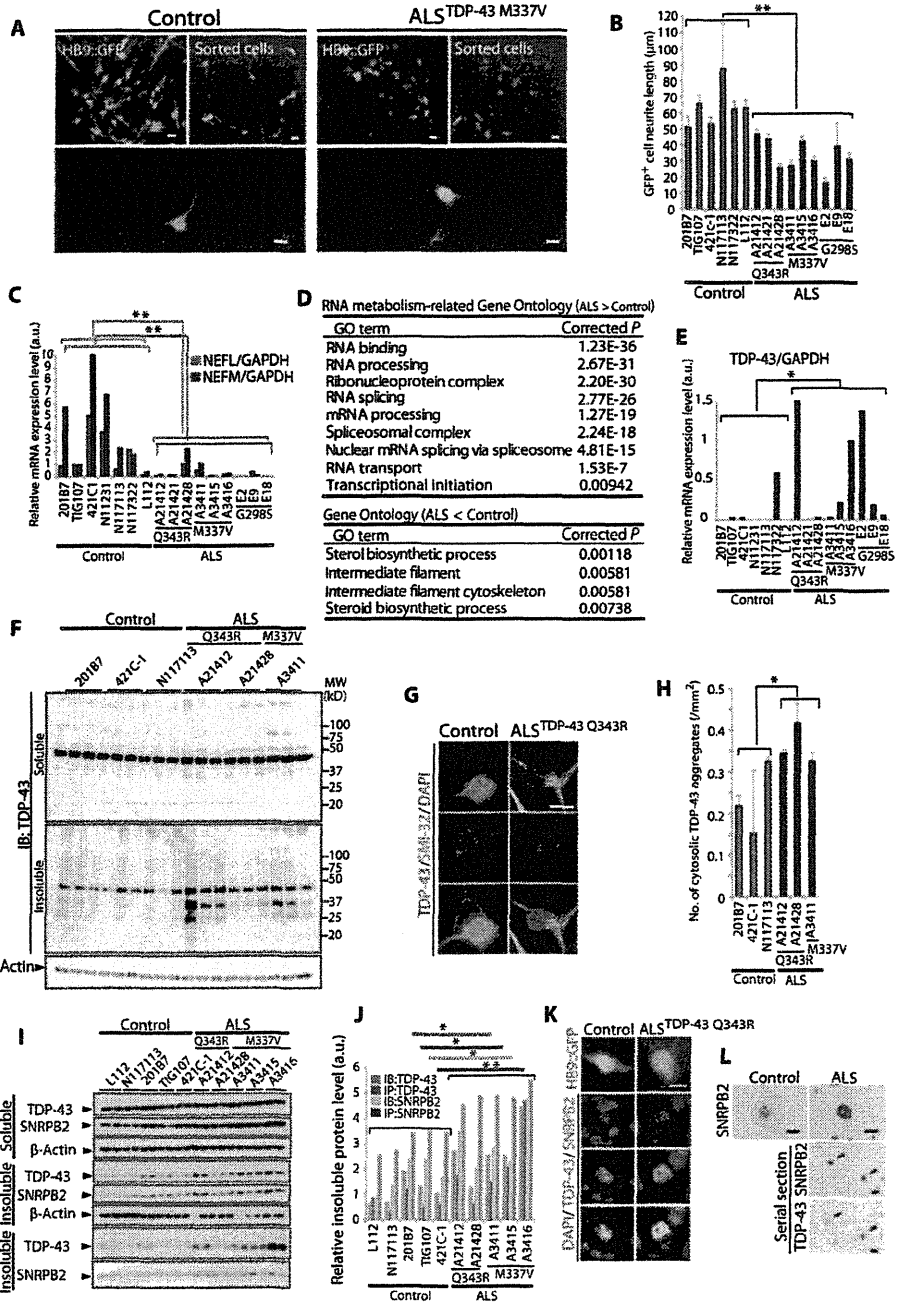

Fig. 2. Phenotypes of ALS iPSC–derived motor neurons. (**A**) ALS iPSC–derived HB9::GFP-positive motor neurons are shown before and after sorting by FACS. (Lower panels) Representative images of purified ALS and control iPSC–derived motor neurons. Scale bars, 10 μm. (**B**) The length of neurites was measured in purified ALS and control iPSC–derived motor neurons. $P = 2.0 \times 10^{-4}$ by t test. Error bars are SEM. (**C**) The expression of NEFL and NEFM was decreased in ALS versus control iPSC–derived motor neurons. $P = 7.9 \times 10^{-3}$, NEFL; $P = 5.3 \times 10^{-3}$, NEFM by t test. (**D**) Major GO terms showed both increases and decreases in gene expression in ALS versus control iPSC–derived motor neurons. (**E**) qPCR showed increased expression of TDP-43 mRNA relative to glyceraldehyde-3-phosphate dehydrogenase (GAPDH) mRNA in ALS versus control iPSC–derived motor neurons. $P = 0.040$ by t test. (**F**) Soluble (upper panel) and insoluble (lower panel) TDP-43 fractions from ALS and control iPSC–derived motor neuron–containing neural populations. (**G**) ALS and control iPSC–derived motor neurons were immunostained for TDP-43 and for the SMI-32 motor neuron marker; DAPI nuclear stain, blue. Scale bars, 10 μm. (**H**) Number of TDP-43–positive cytosolic aggregates measured by high-content analysis. $P = 0.0458$ by t test. Error bars are SEM. (**I**) Immunoblots of different proteins including TDP-43 with antibodies against indicated proteins. Insoluble TDP-43 was immunoprecipitated (IP) from the insoluble fraction and immunoblotted (IB) with each antibody. (**J**) Quantification of protein band densities of TDP-43 and SNRPB2 in insoluble fractions from total lysates and in TDP-43–immunoprecipitated insoluble fractions relative to β-actin. $P = 0.034$ (TDP-43 in the insoluble fraction from total lysates of ALS compared to control motor neuron–containing neural populations) by t test; $P = 1.0 \times 10^{-4}$ (SNRPB2 coimmunoprecipitated with TDP-43 in ALS compared to control motor neuron–containing neural populations) by t test. (**K**) HB9::GFP-labeled ALS and control iPSC–derived motor neurons were immunostained for SNRPB2 and TDP-43 and counterstained with DAPI nuclear stain (blue). Scale bar, 10 μm. (**L**) Representative images showing immunostaining for SNRPB2 in postmortem spinal cord tissue from ALS patients or control individuals. Arrowheads, ALS spinal cord tissue immunoreactive for both TDP-43 and SNRPB2 in serial sections. Scale bars, 10 μm. $^*P < 0.05$, $^{**}P < 0.01$.

iPSC-derived motor neurons was mainly localized in the nucleus, whereas TDP-43 in ALS iPSC-derived motor neurons was distributed in both the nucleus and the cytoplasm (Fig. 2G), with TDP-43 in the cytoplasm forming preinclusion-like aggregates. High-content analysis revealed that the number of such TDP-43 aggregates in ALS motor neurons was increased compared to that in control motor neurons ($P = 0.0458$ by t test; Fig. 2H).

Next, we analyzed SNRPB2, a highly expressed spliceosomal factor, in ALS iPSC-derived motor neurons (fig. S8E). The amount of TDP-43 protein was increased ($P = 0.034$ by t test; Fig. 2, I and J), and the amount of SNRPB2 bound to TDP-43 was increased ($P = 1.0 \times 10^{-4}$ by t test; Fig. 2, I and J) in the insoluble fraction of ALS iPSC-derived motor neuron–containing neural populations compared to control. TDP-43 colocalized with SNRPB2 to form aggregates in the nucleus of ALS iPSC-derived motor neurons (Fig. 2K) and motor neurons from postmortem tissue from ALS patients (Fig. 2L).

Next, we established an assay to measure death of ALS iPSC-derived motor neurons in response to arsenite, which induces oxidative stress and an increase in the amount of insoluble TDP-43 in these motor neurons (*25*). Arsenite increased the amount of TDP-43 in the insoluble fraction of ALS iPSC-derived motor neuron–containing neural populations [$P = 7.8 \times 10^{-3}$ by two-way analysis of variance (ANOVA); Fig. 3, A and B]. The number of surviving ALS iPSC-derived motor neurons was lower compared to control iPSC-derived motor neurons (18% reduction in ALS motor neurons relative to control; $P = 5.0 \times 10^{-4}$ by two-way ANOVA) (Fig. 3, C and D). Staining with ethidium homodimer-1, which selectively permeates the broken membranes of dying cells, revealed that the proportion of dying ALS iPSC-derived motor neurons was greater than that of control iPSC-derived motor neurons [33.5 ± 1.9% (mean ± SD) for ALS compared to 16.1 ± 3.0% for control; $P = 2.9 \times 10^{-3}$ by two-way ANOVA] (Fig. 3, E and F).

Given that gene expression analysis suggested that transcription and RNA splicing were perturbed in ALS iPSC-derived motor neurons, we tested four drugs that had been reported to modulate transcription through histone modification or RNA

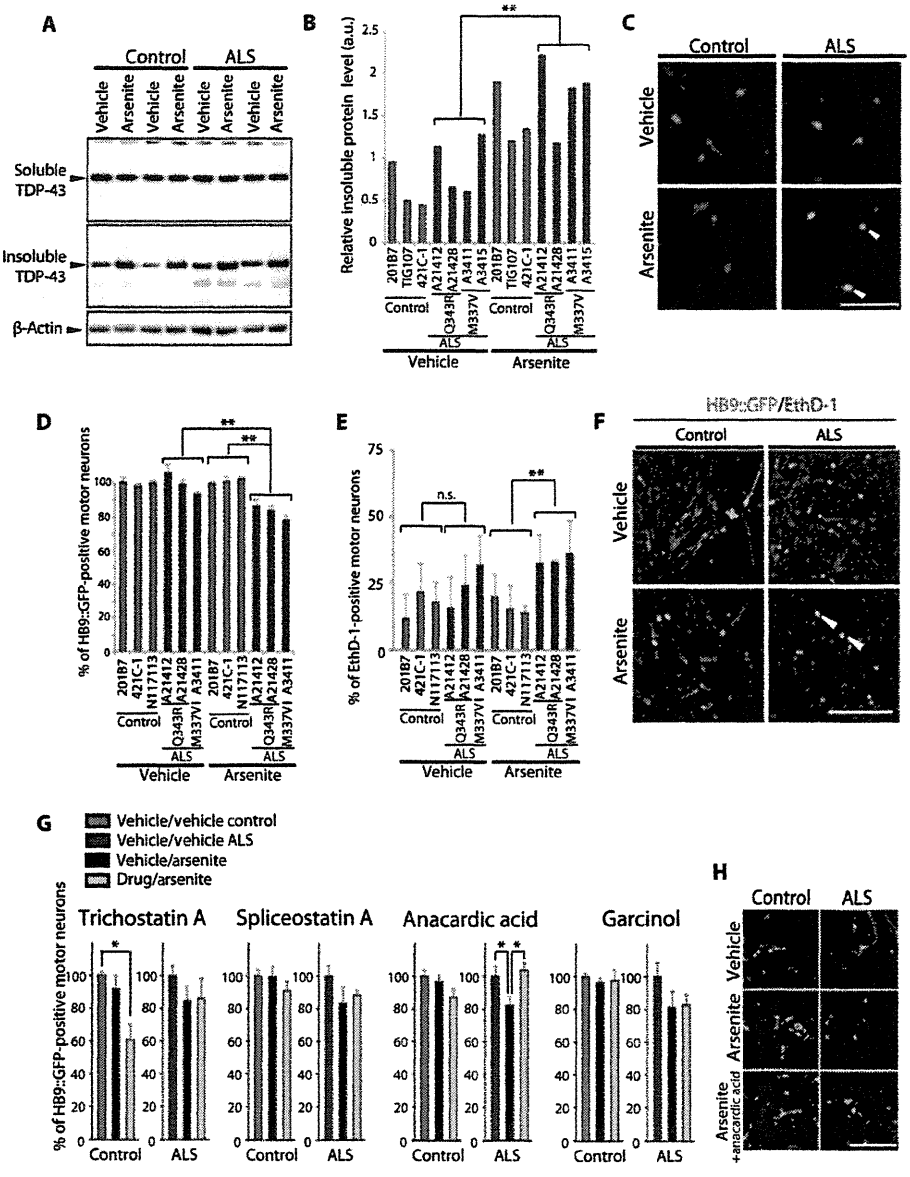

Fig. 3. Arsenite-induced death of ALS and control iPSC-derived motor neurons. (**A** and **B**) Decreased solubility of TDP-43 after treatment with arsenite. (A) After treatment with vehicle or arsenite (0.5 mM, 1 hour), cell lysates were separated into soluble and insoluble fractions and immunoblotted with TDP-43 antibody. (B) Arsenite increased the amount of TDP-43 in the insoluble fraction in ALS iPSC-derived motor neurons ($n = 4$) compared to control ($n = 3$). $P = 7.8 \times 10^{-3}$ by two-way ANOVA. (**C**) Images of control versus ALS iPSC-derived motor neurons after treatment with vehicle or arsenite. Arrowheads, dying motor neurons. Scale bar, 100 μm. (**D**) Proportion of HB9::GFP-positive control and ALS iPSC-derived motor neurons after treatment with vehicle or arsenite. $P = 5.0 \times 10^{-4}$ by two-way ANOVA. Error bars are SEM. (**E**) Death of motor neurons was assessed by ethidium homodimer-1 (EthD-1) uptake after incubation with vehicle or arsenite. $P = 2.9 \times 10^{-3}$ by two-way ANOVA. Error bars are SEM. (**F**) Images of ALS versus control iPSC-derived motor neurons after arsenite treatment. Scale bar, 100 μm. (**G**) Treatment with 5 μM anacardic acid ($n = 6$) for 16 hours blocked arsenite-induced death of ALS iPSC-derived motor neurons. Trichostatin A (3 μM) ($n = 3$), spliceostatin A (100 ng/ml) ($n = 3$), and garcinol (5 μM) ($n = 6$) failed to block arsenite-induced cell death. $P = 0.048$ by one-way ANOVA. Error bars are SEM. (**H**) Images of anacardic acid–treated motor neurons followed by arsenite treatment. Scale bar, 100 μm. $^*P < 0.05$, $^{**}P < 0.01$.

splicing in the arsenite-induced motor neuron death assay. The drugs were trichostatin A (a histone deacetyltransferase inhibitor), spliceostatin A (a spliceosomal factor inhibitor) (*26*), and two histone acetyltransferase inhibitors, anacardic acid (*27*) and garcinol (*27*). We identified anacardic acid as protecting against arsenite-induced death of ALS iPSC–derived motor neurons [survival rate, 81.7 ± 4.5% (mean ± SEM) for arsenite-treated ALS motor neurons compared to 97.1 ± 4.8% for arsenite-treated ALS motor neurons pretreated with anacardic acid; $P = 0.048$ by one-way ANOVA] (Fig. 3, G and H).

Anacardic acid decreased TDP-43 mRNA expression in ALS iPSC–derived motor neurons by 147-fold compared to untreated motor neurons ($P = 0.047$ by two-way ANOVA) (Fig. 4A). To investigate the effect of anacardic acid on the production of TDP-43 protein, we treated ALS iPSC–derived motor neuron–containing neural populations with anacardic acid for 48 hours. Anacardic acid reduced the amount of TDP-43 in the insoluble fraction but not in the soluble fraction of ALS iPSC–derived motor neuron–containing neural populations ($P = 8.2 \times 10^{-3}$ by *t* test) (Fig. 4, B and C). Anacardic acid also increased the length of neurites of purified ALS iPSC–derived motor neurons compared to untreated ALS iPSC–derived motor neurons [average neurite length, 75.4 ± 7.5 μm (mean ± SEM) for anacardic acid–treated ALS motor neurons compared to 36.2 ± 2.5 μm for vehicle-treated ALS motor neurons; $P = 0.014$ by two-way ANOVA] (Fig. 4D and fig. S9C). The drug also increased expression of NEFM mRNA (Fig. 4E), down-regulated expression of RNA metabolism–related genes (Fig. 4F), and reversed changes in the tumor necrosis factor–α (TNFα)/nuclear factor κB (NF-κB) signaling pathway (Fig. 4G and fig. S10, A to D).

DISCUSSION

We found cellular and molecular phenotypes associated with ALS in motor neurons derived from ALS patient–specific iPSCs harboring mutant TDP-43. Consistent with a previous study describing the generation of iPSCs from ALS patients carrying the TDP-43 M337V mutation (*13*), in our study, the TDP-43 mutation did not affect the differentiation of ALS iPSCs into motor neurons. We report an increase in insoluble TDP-43 in motor neuron–containing neural populations differentiated from ALS patient-derived iPSCs. We also observed a punctate cytoplasmic distribution of TDP-43 in ALS iPSC–derived motor neurons and a cellular vulnerability to arsenite treatment, in agreement with the previous report, which showed increased vulnerability of ALS motor neurons to other

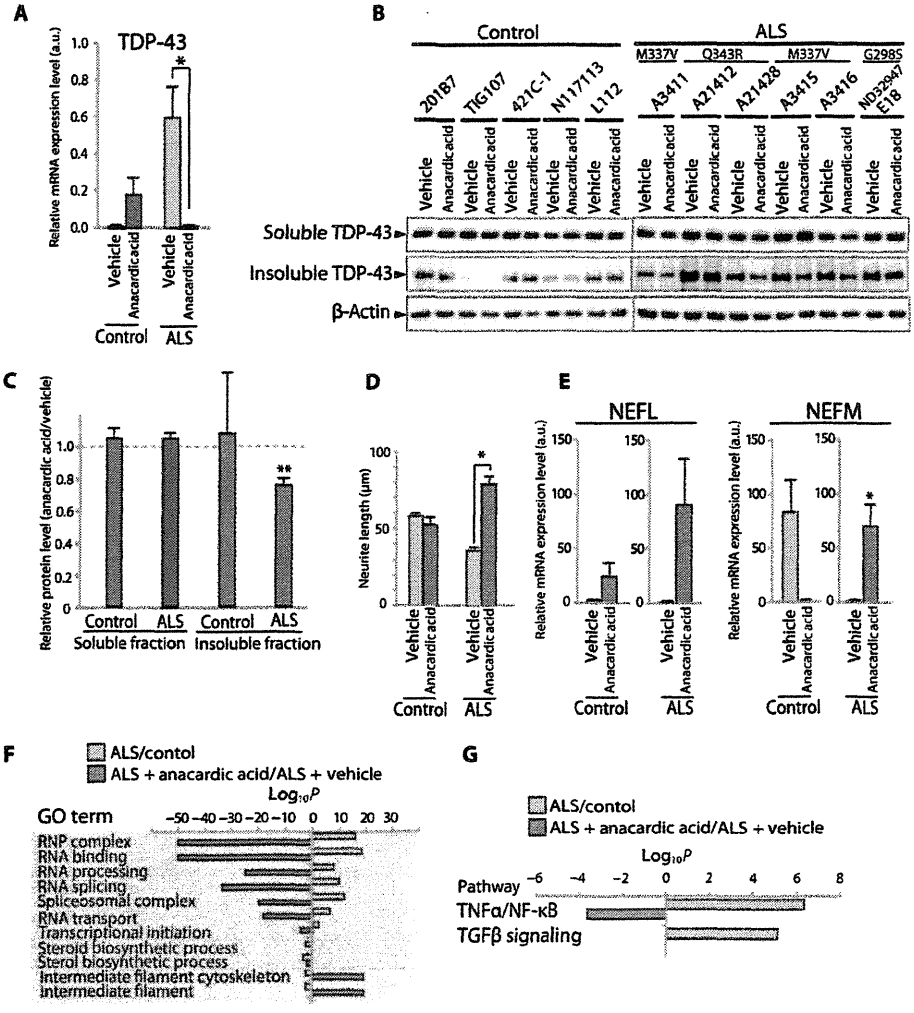

Fig. 4. Anacardic acid–induced phenotypic changes in ALS and control motor neurons. (**A**) qPCR confirmed that 5 μM anacardic acid treatment for 16 hours down-regulated TDP-43 mRNA expression in purified ALS iPSC–derived motor neurons. $P = 0.047$ by two-way ANOVA. Error bars are SEM. (**B**) After treatment with vehicle or 5 μM anacardic acid for 48 hours, cells were lysed, separated into soluble and insoluble fractions, and immunoblotted with TDP-43. (**C**) Quantification of protein band densities after immunoblotting. The dotted line indicates the baseline (vehicle only) of relative protein levels (anacardic acid/vehicle). $P = 8.2 \times 10^{-3}$ by *t* test. Error bars are SEM. (**D**) Neurite length of purified motor neurons was measured 16 hours after treatment with vehicle or 5 μM anacardic acid. $P = 0.014$ by two-way ANOVA. Error bars are SEM. (**E**) qPCR revealed that anacardic acid treatment up-regulated expression of NEFM mRNA in ALS iPSC–derived motor neurons. $P = 0.032$ by *t* test. Error bars are SEM. (**F** and **G**) After purified motor neurons were treated for 16 hours with vehicle or 5 μM anacardic acid, cells were lysed and analyzed by expression array profiling. (Yellow bars) *P* value for significant changes in expression of genes and signaling pathways in ALS versus control iPSC–derived motor neurons was expressed on a logarithmic scale. (Green bars) *P* value for GO terms and signaling pathways of anacardic acid–treated ALS motor neurons compared to vehicle-treated ALS motor neurons was expressed on a logarithmic scale. $^*P < 0.05$, $^{**}P < 0.01$. TGFβ, transforming growth factor–β.

cellular stressors (*13*). There were, however, two differences between these studies. In the previous study (*13*), TDP-43 mRNA expression was similar between control iPSC–derived motor neuron culture and iPSC-derived motor neuron culture from ALS patients with the TDP-43 (M337V) mutation. In contrast, we found that TDP-43 mRNA was up-regulated in ALS iPSC–derived motor neurons with the same TDP-43 M337V mutation or with two other mutations (Q343R and G298S) compared to control iPSC–derived motor neurons. We speculate that there may be several reasons for this difference between the two studies. First, we analyzed multiple iPSC lines to account for clonal variation. We found that in one ALS iPSC line with the TDP-43 M337V mutation, TDP-43 mRNA expression was close to control, whereas the other ALS iPSC lines containing the same mutation showed up-regulation of TDP-43 mRNA. Second, we analyzed the expression of TDP-43 mRNA in purified ALS iPSC–derived motor neurons to avoid contamination with other cell types. Another difference between the two studies was the result of the lactate dehydrogenase cytotoxicity assay (fig. S11). Unlike the previous study, we found no difference in survival between control and ALS motor neurons using this assay. We speculate that this discrepancy stemmed from the fact that we used multiple iPSC lines from three different ALS patients and that this reduced the impact of clonal variation. Further progress in culture methods for motor neurons might make it possible to recapitulate ALS motor neuron death under basal conditions.

In our study, we used multiple iPSC lines from three different ALS patients for our phenotyping assays to address the challenge of clonal variation because we discovered variations even between iPSC lines derived from the same ALS patient. Although we did not use all of the iPSC clones from all ALS patients in all of the assays, we used at least two clones from each ALS patient in each phenotyping assay including immunoblot analysis of insoluble TDP-43, neurite length quantification, and quantitative polymerase chain reaction (qPCR) analysis of TDP-43 mRNA. In the drug screening assay, we used selected ALS iPSC lines and tested a positive hit on phenotyped clones that were not included in the primary screening assay. We demonstrated that the results of drug screening were not specific to the subset of screened clones. Clonal variation of iPSC lines continues to be an obstacle for cellular modeling of disease.

We found that mutant TDP-43 was more insoluble and more prone to forming aggregates than wild-type TDP-43. These properties may contribute to loss of the negative feedback loop that autoregulates synthesis of TDP-43 (*8*), which could in turn lead to increased expression of TDP-43 mRNA and protein. Increased amounts of TDP-43 protein bound to other RNA binding proteins such as the spliceosomal factor SNRPB2 could lead to perturbation of RNA metabolism. We generated iPSCs from three ALS patients carrying distinct TDP-43 mutations: Q343R, M337V, and G298S. These mutations and other mutations are located in the glycine-rich domain of TDP-43 (*28*). We speculate that mutations in the glycine-rich domain of TDP-43 may disrupt the interaction of mutant TDP-43 with other proteins or RNAs, leading to up-regulation of TDP-43 mRNA, an increase in mutant TDP-43 protein, and the formation of more aggregates. In our study, mutant TDP-43 was more sensitive to oxidative stress, which increased the amount of insoluble TDP-43 and hence aggregate formation. Anacardic acid may reverse ALS-associated phenotypes potentially by down-regulation of TDP-43 mRNA expression. However, anacardic acid might partially exert its effect through the suppression of other genes that are regulated by NF-κB (*29*) or through control of redox signaling (*30*) because pathogenic TDP-43 has been implicated in both pathways (*23*, *25*).

In summary, we identified cellular and molecular phenotypes associated with ALS using ALS patient–specific iPSC–derived motor neurons and set up a screening assay that identified anacardic acid as a drug that could reverse some of the ALS phenotypes. Our data suggest that ALS iPSC–derived motor neurons may be useful for elucidating disease pathogenesis and for identifying new candidate drugs.

MATERIALS AND METHODS

Derivation of patient-specific fibroblasts

Control and ALS-derived human dermal fibroblasts (HDFs) other than ND32947 were generated from explants of 3-mm dermal biopsies. ND32947 was obtained from Coriell Institute (Camden, NJ). After 1 to 2 weeks, fibroblast outgrowths from the explants were passaged.

iPSC generation

Human complementary DNAs for reprogramming factors were transduced in HDF with retrovirus (Sox2, Klf4, Oct3/4, and/or c-Myc) or episomal vectors (Sox2, Klf4, Oct3/4, L-Myc, Lin28, short hairpin RNA for p53). Several days after transduction, fibroblasts were harvested and replated on an SNL feeder layer. On the next day, the medium was changed to primate embryonic stem cell medium (ReproCELL) supplemented with basic fibroblast growth factor (4 ng/ml) (Wako Chemicals). The medium was changed every other day. Thirty days after transduction, iPSC colonies were picked up.

Immunocytochemistry

Cells were fixed in 4% paraformaldehyde (pH 7.4) for 30 min at room temperature and rinsed with phosphate-buffered saline (PBS). The cells were permeabilized in PBS containing 0.2% Triton X-100 for 10 min at room temperature, followed by rinsing with PBS. Nonspecific binding was blocked with PBS containing 10% donkey serum for 60 min at room temperature. Cells were incubated with primary antibodies overnight at 4°C and then labeled with appropriate fluorescently tagged secondary antibodies. DAPI (4′,6-diamidino-2-phenylindole) (Life Technologies) was used to label nuclei. Fluorescence images were acquired on DeltaVision (Applied Precision). The following primary antibodies were used in this assay: Nanog (R&D Systems, 1:10), SSEA-4 (Millipore, 1:100), SOX-17 (R&D Systems, 1:50), αSMA (DAKO A/S, 1:500), Tuj1 (Covance, 1:2000), Islet-1 (Developmental Studies Hybridoma Bank, 1:50), HB9 (Epitomics, 1:2000), ChAT (Millipore, 1:100), SMI-32 (Covance, 1:500), synapsin (Millipore, 1:500), MAP2 (Millipore, 1:200), GFAP (DAKO, 1:1000), TDP-43 (Proteintech, 1:500), and SNRPB2 (Proteintech, 1:300).

Quantitating the number of TDP-43 aggregates in cytoplasm

Differentiated motor neurons were visualized with anti–SMI-32 antibody. Nuclei were then stained with DAPI. The number of TDP-43 dots in cytoplasm was quantified by IN Cell Analyzer 6000 (GE Healthcare). The TDP-43 dot was defined by a size of more than 0.324 μm.

Immunoprecipitation

After being washed with PBS, cells cultured in 24-well plates were solubilized for 30 min on ice in immunoprecipitation assay buffer

(50 mM tris-HCl, 150 mM NaCl, 1 mM EDTA, 1% Triton X-100, 0.1% SDS, and 0.1% sodium deoxycholate) with a protease inhibitor cocktail and a phosphatase inhibitor with Bioruptor (high mode, ON: 30 s, OFF: 60 s, 20 times). Insoluble fraction was collected by centrifugation (15,000 rpm, 3 min), in which the supernatant was defined as soluble fraction, and lysed in SDS lysis solution (50 mM tris-HCl, 10 mM EDTA, 1% SDS) with Bioruptor. Soluble lysates were incubated overnight with protein G–Sepharose bound to anti–TDP-43 antibody (Abnova). Lysates from insoluble fraction were diluted to 10% by dilution buffer (50 mM tris-HCl, 167 mM NaCl, 1.1% Triton X-100, and 0.11% sodium deoxycholate) including phosphatase inhibitor and then incubated overnight by protein G–Sepharose bound to anti–TDP-43 antibody (Abnova). Sepharose beads were collected by brief centrifugation and washed with TBS buffer (50 mM tris-HCl, 150 mM NaCl, pH 7.4) three times. Immunoprecipitated material was eluted by boiling for 3 min in 2× sample buffer [125 mM tris-HCl (pH 6.8), 4% SDS, 20% glycerol, 0.004% bromophenol blue].

Induction of motor neurons by quick embryoid body–like aggregate method (SFEBq)

Human iPSCs were dissociated to single cells and quickly reaggregated in low cell adhesion U-shaped 96-well plates (Lipidure-Coat Plate A-U96, NOF Corporation). Aggregations were cultured in 5% DFK medium [5% KSR Medium (DFK5%), Dulbecco's modified Eagle's medium/Ham's F12 (Sigma-Aldrich), 5% KSR (Invitrogen), minimum essential medium–nonessential amino acids (Invitrogen), L-glutamine (Sigma-Aldrich), 2-mercaptoethanol (Wako)] with 2 μM dorsomorphin and SB431542 in a neural inductive stage (P1) for 12 days. After patterning with neurobasal medium supplemented with B27, 1 μM retinoic acid, Sonic Hedgehog (100 to 500 ng/ml), and fibroblast growth factor 2 (12.5 ng/ml), the aggregates were adhered to Matrigel (BD Biosciences)–coated dishes on day 22. Adhesive embryoid bodies were cultured in neurobasal medium with brain-derived neurotrophic factor (10 ng/ml), glial cell line–derived neurotrophic factor (10 ng/ml), and NT-3 (10 ng/ml) in P2 culture. They were separated from the dish by Accutase, dissociated into a small clump or single cells, and cultured at 500,000 cells per well on Matrigel-coated 24-well dishes on day 35 as P3 maturation stage.

SUPPLEMENTARY MATERIALS

www.sciencetranslationalmedicine.org/cgi/content/full/4/145/145ra104/DC1
Materials and Methods
Fig. S1. ESC marker, genotype, and karyotype analysis.
Fig. S2. Transgene expression.
Fig. S3. In vitro three-germ layer and teratoma assay.
Fig. S4. Bisulfite genomic sequencing of the promoter regions of Nanog and Oct4.
Fig. S5. Comparison of global gene expression profiles of human iPSCs.
Fig. S6. Motor neuron differentiation and functional assay of motor neurons.
Fig. S7. Estimation of neuronal differentiation from control and ALS iPSCs.
Fig. S8. Motor neuron purification for gene expression analysis.
Fig. S9. Decreased neurite length of ALS motor neurons.
Fig. S10. Signaling pathways significantly activated in ALS motor neurons.
Fig. S11. Cell viability and cytotoxicity.
Table S1. List of clones for human iPSC lines.
Table S2. Correlation coefficients of global gene expression in human iPSC lines.
Table S3. GO analysis of microarray data (fold change >1.2) ALS UP.
Table S4. GO analysis of microarray data (fold change >1.2) ALS DOWN.
Table S5. Genes identified as significantly increased ($P < 0.05$) with >1.2-fold change in motor neurons derived from ALS human iPSCs.
Table S6. Genes identified as significantly decreased ($P < 0.05$) with >1.2-fold change in motor neurons derived from ALS human iPSCs.
Table S7. Primers list.
References

REFERENCES AND NOTES

1. L. I. Bruijn, T. M. Miller, D. W. Cleveland, Unraveling the mechanisms involved in motor neuron degeneration in ALS. *Annu. Rev. Neurosci.* **27**, 723–749 (2004).
2. J. D. Rothstein, Current hypotheses for the underlying biology of amyotrophic lateral sclerosis. *Ann. Neurol.* **65** (Suppl. 1), S3–S9 (2009).
3. M. Neumann, D. M. Sampathu, L. K. Kwong, A. C. Truax, M. C. Micsenyi, T. T. Chou, J. Bruce, T. Schuck, M. Grossman, C. M. Clark, L. F. McCluskey, B. L. Miller, E. Masliah, I. R. Mackenzie, H. Feldman, W. Feiden, H. A. Kretzschmar, J. Q. Trojanowski, V. M. Lee, Ubiquitinated TDP-43 in frontotemporal lobar degeneration and amyotrophic lateral sclerosis. *Science* **314**, 130–133 (2006).
4. T. Arai, M. Hasegawa, H. Akiyama, K. Ikeda, T. Nonaka, H. Mori, D. Mann, K. Tsuchiya, M. Yoshida, Y. Hashizume, T. Oda, TDP-43 is a component of ubiquitin-positive tau-negative inclusions in frontotemporal lobar degeneration and amyotrophic lateral sclerosis. *Biochem. Biophys. Res. Commun.* **351**, 602–611 (2006).
5. I. R. Mackenzie, E. H. Bigio, P. G. Ince, F. Geser, M. Neumann, N. J. Cairns, L. K. Kwong, M. S. Forman, J. Ravits, H. Stewart, A. Eisen, L. McClusky, H. A. Kretzschmar, C. M. Monoranu, J. R. Highley, J. Kirby, T. Siddique, P. J. Shaw, V. M. Lee, J. Q. Trojanowski, Pathological TDP-43 distinguishes sporadic amyotrophic lateral sclerosis from amyotrophic lateral sclerosis with *SOD1* mutations. *Ann. Neurol.* **61**, 427–434 (2007).
6. E. Kabashi, L. Lin, M. L. Tradewell, P. A. Dion, V. Bercier, P. Bourgouin, D. Rochefort, S. Bel Hadj, H. D. Durham, C. Vande Velde, G. A. Rouleau, P. Drapeau, Gain and loss of function of ALS-related mutations of *TARDBP* (TDP-43) cause motor deficits in vivo. *Hum. Mol. Genet.* **19**, 671–683 (2010).
7. M. J. Strong, The evidence for altered RNA metabolism in amyotrophic lateral sclerosis (ALS). *J. Neurol. Sci.* **288**, 1–12 (2010).
8. Y. M. Ayala, L. De Conti, S. E. Avendaño-Vázquez, A. Dhir, M. Romano, A. D'Ambrogio, J. Tollervey, J. Ule, M. Baralle, E. Buratti, F. E. Baralle, TDP-43 regulates its mRNA levels through a negative feedback loop. *EMBO J.* **30**, 277–288 (2011).
9. L. Liu-Yesucevitz, A. Bilgutay, Y. J. Zhang, T. Vanderweyde, A. Citro, T. Mehta, N. Zaarur, A. McKee, R. Bowser, M. Sherman, L. Petrucelli, B. Wolozin, Tar DNA binding protein-43 (TDP-43) associates with stress granules: Analysis of cultured cells and pathological brain tissue. *PLoS One* **5**, e13250 (2010).
10. N. J. Rutherford, Y. J. Zhang, M. Baker, J. M. Gass, N. A. Finch, Y. F. Xu, H. Stewart, B. J. Kelley, K. Kuntz, R. J. Crook, J. Sreedharan, C. Vance, E. Sorenson, C. Lippa, E. H. Bigio, D. H. Geschwind, D. S. Knopman, H. Mitsumoto, R. C. Petersen, N. R. Cashman, M. Hutton, C. E. Shaw, K. B. Boylan, B. Boeve, N. R. Graff-Radford, Z. K. Wszolek, R. J. Caselli, D. W. Dickson, I. R. Mackenzie, L. Petrucelli, R. Rademakers, Novel mutations in *TARDBP* (TDP-43) in patients with familial amyotrophic lateral sclerosis. *PLoS Genet.* **4**, e1000193 (2008).
11. H. Inoue, S. Yamanaka, The use of induced pluripotent stem cells in drug development. *Clin. Pharmacol. Ther.* **89**, 655–661 (2011).
12. J. T. Dimos, K. T. Rodolfa, K. K. Niakan, L. M. Weisenthal, H. Mitsumoto, W. Chung, G. F. Croft, G. Saphier, R. Leibel, R. Goland, H. Wichterle, C. E. Henderson, K. Eggan, Induced pluripotent stem cells generated from patients with ALS can be differentiated into motor neurons. *Science* **321**, 1218–1221 (2008).
13. B. Bilican, A. Serio, S. J. Barmada, A. L. Nishimura, G. J. Sullivan, M. Carrasco, H. P. Phatnani, C. A. Puddifoot, D. Story, J. Fletcher, I. H. Park, B. A. Friedman, G. Q. Daley, D. J. Wyllie, G. E. Hardingham, I. Wilmut, S. Finkbeiner, T. Maniatis, C. E. Shaw, S. Chandran, Mutant induced pluripotent stem cell lines recapitulate aspects of TDP-43 proteinopathies and reveal cell-specific vulnerability. *Proc. Natl. Acad. Sci. U.S.A.* **109**, 5803–5808 (2012).
14. K. Takahashi, K. Tanabe, M. Ohnuki, M. Narita, T. Ichisaka, K. Tomoda, S. Yamanaka, Induction of pluripotent stem cells from adult human fibroblasts by defined factors. *Cell* **131**, 861–872 (2007).
15. K. Okita, Y. Matsumura, Y. Sato, A. Okada, A. Morizane, S. Okamoto, H. Hong, M. Nakagawa, K. Tanabe, K. Tezuka, T. Shibata, T. Kunisada, M. Takahashi, J. Takahashi, H. Saji, S. Yamanaka, A more efficient method to generate integration-free human iPS cells. *Nat. Methods* **8**, 409–412 (2011).
16. T. Wada, M. Honda, I. Minami, N. Tooi, Y. Amagai, N. Nakatsuji, K. Aiba, Highly efficient differentiation and enrichment of spinal motor neurons derived from human and monkey embryonic stem cells. *PLoS One* **4**, e6722 (2009).
17. M. C. Marchetto, A. R. Muotri, Y. Mu, A. M. Smith, G. G. Cezar, F. H. Gage, Non-cell-autonomous effect of human $SOD1^{G37R}$ astrocytes on motor neurons derived from human embryonic stem cells. *Cell Stem Cell* **3**, 649–657 (2008).
18. C. Bergeron, K. Beric-Maskarel, S. Muntasser, L. Weyer, M. J. Somerville, M. E. Percy, Neurofilament light and polyadenylated mRNA levels are decreased in amyotrophic lateral sclerosis motor neurons. *J. Neuropathol. Exp. Neurol.* **53**, 221–230 (1994).

19. K. Watanabe, D. Kamiya, A. Nishiyama, T. Katayama, S. Nozaki, H. Kawasaki, Y. Watanabe, K. Mizuseki, Y. Sasai, Directed differentiation of telencephalic precursors from embryonic stem cells. *Nat. Neurosci.* **8**, 288–296 (2005).
20. E. B. Lee, V. M. Lee, J. Q. Trojanowski, Gains or losses: Molecular mechanisms of TDP43-mediated neurodegeneration. *Nat. Rev. Neurosci.* **13**, 38–50 (2012).
21. J. R. Tollervey, T. Curk, B. Rogelj, M. Briese, M. Cereda, M. Kayikci, J. König, T. Hortobágyi, A. L. Nishimura, V. Zupunski, R. Patani, S. Chandran, G. Rot, B. Zupan, C. E. Shaw, J. Ule, Characterizing the RNA targets and position-dependent splicing regulation by TDP-43. *Nat. Neurosci.* **14**, 452–458 (2011).
22. M. Polymenidou, C. Lagier-Tourenne, K. R. Hutt, S. C. Huelga, J. Moran, T. Y. Liang, S. C. Ling, E. Sun, E. Wancewicz, C. Mazur, H. Kordasiewicz, Y. Sedaghat, J. P. Donohue, L. Shiue, C. F. Bennett, G. W. Yeo, D. W. Cleveland, Long pre-mRNA depletion and RNA missplicing contribute to neuronal vulnerability from loss of TDP-43. *Nat. Neurosci.* **14**, 459–468 (2011).
23. V. Swarup, D. Phaneuf, N. Dupré, S. Petri, M. Strong, J. Kriz, J. P. Julien, Deregulation of TDP-43 in amyotrophic lateral sclerosis triggers nuclear factor κB–mediated pathogenic pathways. *J. Exp. Med.* **208**, 2429–2447 (2011).
24. W. Guo, Y. Chen, X. Zhou, A. Kar, P. Ray, X. Chen, E. J. Rao, M. Yang, H. Ye, L. Zhu, J. Liu, M. Xu, Y. Yang, C. Wang, D. Zhang, E. H. Bigio, M. Mesulam, Y. Shen, Q. Xu, K. Fushimi, J. Y. Wu, An ALS-associated mutation affecting TDP-43 enhances protein aggregation, fibril formation and neurotoxicity. *Nat. Struct. Mol. Biol.* **18**, 822–830 (2011).
25. T. J. Cohen, A. W. Hwang, T. Unger, J. Q. Trojanowski, V. M. Lee, Redox signalling directly regulates TDP-43 via cysteine oxidation and disulphide cross-linking. *EMBO J.* **31**, 1241–1252 (2011).
26. D. Kaida, H. Motoyoshi, E. Tashiro, T. Nojima, M. Hagiwara, K. Ishigami, H. Watanabe, T. Kitahara, T. Yoshida, H. Nakajima, T. Tani, S. Horinouchi, M. Yoshida, Spliceostatin A targets SF3b and inhibits both splicing and nuclear retention of pre-mRNA. *Nat. Chem. Biol.* **3**, 576–583 (2007).
27. F. J. Dekker, H. J. Haisma, Histone acetyl transferases as emerging drug targets. *Drug Discov. Today* **14**, 942–948 (2009).
28. G. S. Pesiridis, V. M. Lee, J. Q. Trojanowski, Mutations in TDP-43 link glycine-rich domain functions to amyotrophic lateral sclerosis. *Hum. Mol. Genet.* **18**, R156–R162 (2009).
29. B. Sung, M. K. Pandey, K. S. Ahn, T. Yi, M. M. Chaturvedi, M. Liu, B. B. Aggarwal, Anacardic acid (6-nonadecyl salicylic acid), an inhibitor of histone acetyltransferase, suppresses expression of nuclear factor-κB–regulated gene products involved in cell survival, proliferation, invasion, and inflammation through inhibition of the inhibitory subunit of nuclear factor-κBα kinase, leading to potentiation of apoptosis. *Blood* **111**, 4880–4891 (2008).
30. M. Toyomizu, K. Okamoto, T. Ishibashi, Z. Chen, T. Nakatsu, Uncoupling effect of anacardic acids from cashew nut shell oil on oxidative phosphorylation of rat liver mitochondria. *Life Sci.* **66**, 229–234 (2000).

Acknowledgments: We thank our co-workers and collaborators; S. L. Pfaff for providing plasmids; M. Kawada, Y. Karatsu, and T. Enami for technical assistance; and K. Murai for editing the manuscript. **Funding:** This research was funded in part by a grant from the Funding Program for World-Leading Innovative R&D on Science and Technology (FIRST Program) of the Japan Society for the Promotion of Science (S. Yamanaka), a grant from the JST Yamanaka iPS cell special project (S. Yamanaka and H. Inoue), Core Research for Evolutional Science and Technology (H. Inoue), Grant-in-Aid from the Ministry of Health and Labour (R.T. and H. Inoue), a Grant-in-Aid for Scientific Research on Innovative Area "Foundation of Synapse and Neurocircuit Pathology" (22110007) from the Ministry of Education, Culture, Sports, Science and Technology of Japan (H. Inoue), and a research grant from the Novartis Foundation for Gerontological Research (H. Inoue). **Author contributions:** H. Inoue planned the project; H. Inoue, N.E., and S.K. designed the experiments; S. Yamanaka, H. Inoue, N.E., and S.K. wrote the manuscript; K.Y., S. Yamawaki, M.N., S.S., K.M., K. Okamoto, H.T., A.T., K.H., and R.T. recruited patients; N.E., S.K., K. Takahashi, K.M., F.A., K.Y., T. Kondo, K. Tsukita, K. Okita, I.A., H. Inoue, and S. Yamanaka generated and characterized iPSCs; T. Aoi conducted karyotyping; A.W. performed methylation analysis of iPSCs; Y.Y. performed immunohistochemical analysis of teratomas; N.E., S.K., K. Takahashi, K.M., and F.A. performed generation and characterization of human motor neurons; A.M. and J.T. provided technical support for neuronal differentiation; D.W. performed whole-cell patch clamp; H.H. and T. Kaneko generated lentivirus vectors with high titers; T.Y. supported the microarray analysis; H. Ito and T. Ayaki performed immunohistochemistry of human spinal cords; M.Y. provided spliceostatin A; A.K. provided human materials; T. Nakahata provided NOG mice; T. Nonaka and M.H. provided antibodies, plasmids, and scientific discussions; R.T. provided scientific discussions; M.C.N.M. and F.H.G. provided plasmids and scientific discussions. **Competing interests:** A.T. is a paid consultant to Chugai Pharmaceutical Co. Ltd. S. Yamanaka is a member of the scientific advisory boards of iPierian, iPS Academia Japan, and Megakaryon Corporation. H. Inoue, N.E., S.K., and K. Tsukita have filed a patent (Prophylactic and therapeutic drug for amyotrophic lateral sclerosis and method of screening, 61/587,323) related to this work. The other authors declare that they have no competing interests.

Submitted 23 March 2012
Accepted 13 July 2012
Published 1 August 2012
10.1126/scitranslmed.3004052

Citation: N. Egawa, S. Kitaoka, K. Tsukita, M. Naitoh, K. Takahashi, T. Yamamoto, F. Adachi, T. Kondo, K. Okita, I. Asaka, T. Aoi, A. Watanabe, Y. Yamada, A. Morizane, J. Takahashi, T. Ayaki, H. Ito, K. Yoshikawa, S. Yamawaki, S. Suzuki, D. Watanabe, H. Hioki, T. Kaneko, K. Makioka, K. Okamoto, H. Takuma, A. Tamaoka, K. Hasegawa, T. Nonaka, M. Hasegawa, A. Kawata, M. Yoshida, T. Nakahata, R. Takahashi, M. C. N. Marchetto, F. H. Gage, S. Yamanaka, H. Inoue, Drug screening for ALS using patient-specific induced pluripotent stem cells. *Sci. Transl. Med.* **4**, 145ra104 (2012).

OPEN ACCESS Freely available online

PLOS | ONE

Methylene Blue Reduced Abnormal Tau Accumulation in P301L Tau Transgenic Mice

Masato Hosokawa[1], Tetsuaki Arai[1,2], Masami Masuda-Suzukake[3], Takashi Nonaka[3], Makiko Yamashita[3], Haruhiko Akiyama[1]*, Masato Hasegawa[3]

1 Department of Dementia and Higher Brain Function, Tokyo Metropolitan Institute of Medical Science, Tokyo, Japan, **2** Department of Psychiatry, Graduate School of Comprehensive Human Sciences, University of Tsukuba, Tsukuba, Japan, **3** Department of Pathology and Cell Biology, Tokyo Metropolitan Institute of Medical Science, Tokyo, Japan

Abstract

In neurodegenerative disorders, abnormally hyperphosphorylated and aggregated tau accumulates intracellularly, a mechanism which is thought to induce neuronal cell death. Methylene blue, a type of phenothiazine, has been reported to inhibit tau aggregation in vitro. However, the effect of methylene blue in vivo has remained unknown. Therefore, we examined whether methylene blue suppresses abnormal tau accumulation using P301L tau transgenic mice. At 8 to 11 months of age, these mice were orally administered methylene blue for 5 months. Subsequent results of Western blotting analysis revealed that this agent reduced detergent-insoluble phospho-tau. Methylene blue may have potential as a drug candidate for the treatment of tauopathy.

Citation: Hosokawa M, Arai T, Masuda-Suzukake M, Nonaka T, Yamashita M, et al. (2012) Methylene Blue Reduced Abnormal Tau Accumulation in P301L Tau Transgenic Mice. PLoS ONE 7(12): e52389. doi:10.1371/journal.pone.0052389

Editor: Andrea C. LeBlanc, McGill University, Canada

Received June 12, 2012; **Accepted** November 14, 2012; **Published** December 20, 2012

Funding: This research was partially supported by the Japan Society for the Promotion of Science, Grants-in-Aid for Scientific Research (C), grant number 21591536 to HA and 24591738 to M. Hosokawa. The additional part of the funding of the authors' study has come from institute budget. The funders had no role in study design, data collection and analysis, decision to publish, or preparation of the manuscript.

Competing Interests: The authors have declared that no competing interests exist.

* E-mail: akiyama-hr@igakuken.or.jp

Introduction

In neurodegenerative disorders such as Alzheimer's disease, corticobasal degeneration, and supranuclear palsy, the microtubule–associated protein tau is abnormally phosphorylated and redistributed into paired helical filaments (PHFs) forming neurofibrillary tangles, a process that correlates with pyramidal cell destruction and dementia. Abnormal tau accumulation is characterized by hyperphosphorylation, conformational change and aggregation with changes in solubility.

Wischik et al. have identified a nonneuroleptic phenothiazine which reverses the proteolytic stability of protease-resistant PHFs by blocking tau-tau binding through the repeat domain [1]. Moreover, phenothiazines, including methylthioninium chloride (methylene blue (MB)), polyphenols and porphyrins, inhibited heparin-induced tau filament formation in vitro [2]. Based on these results, tau aggregation inhibitors are considered to be strong candidates for the treatment of tauopathy.

TauRx Pharmaceuticals recently announced the completion of MB phase II clinical trials. They conducted MB dosing and efficacy studies involving 321 people with mild to moderate Alzheimer's disease. Over a 50-week period, the cognitive decline of those on the drug appeared to be 81% slower than those taking a placebo. These results were presented at a conference [3] but have not been published. Currently, a large-scale phase III trial is in planning [4].

To date, there are two reports on the effect of MB on tau aggregation in vivo. In one study, MB did not alter abnormal tau phosphorylation and failed to inhibit tau-dependent neuronal cell toxicity in zebrafish [5]. The other study employed a distinct tau transgenic mouse line and mice received a 2–3-week treatment with oral MB. In this latter study, MB acted as a tau aggregation inhibitor. Although, these findings have been described in brief in a conference abstract, the details are unavailable [6].

More recently, Congdon et al. demonstrated that MB could induce autophagy in primary neurons, organotypic slice cultures and tau transgenic mice (JNPL3) [7]. They also showed a 2 week oral administration of MB attenuated the total tau levels in the absence of significant changes in sarkosyl-insoluble tau levels.

In the present study, we investigated whether MB could reduce abnormal tau accumulation by carrying out long-term oral administration of MB using tau transgenic mice with the P301L mutation as a tauopathy model. Our results suggested that oral intake of MB could be a potential treatment for tauopathy.

Materials and Methods

Ethics Statement

This study was carried out in strict accordance with the recommendations provided in the Guide for the Care and Use of Laboratory Animals of the Ministry of Health, Labour and Welfare of Japan and the Ministry of Education, Culture, Sports, Science and Technology of Japan. The protocol was approved by the Committee on the Ethics of Animal Experiments of the Tokyo Metropolitan Institute of Medical Science (Permit Numbers: 22–23 and 11-028). All experiments were performed under sodium pentobarbital anesthesia and every effort was made to minimize suffering.

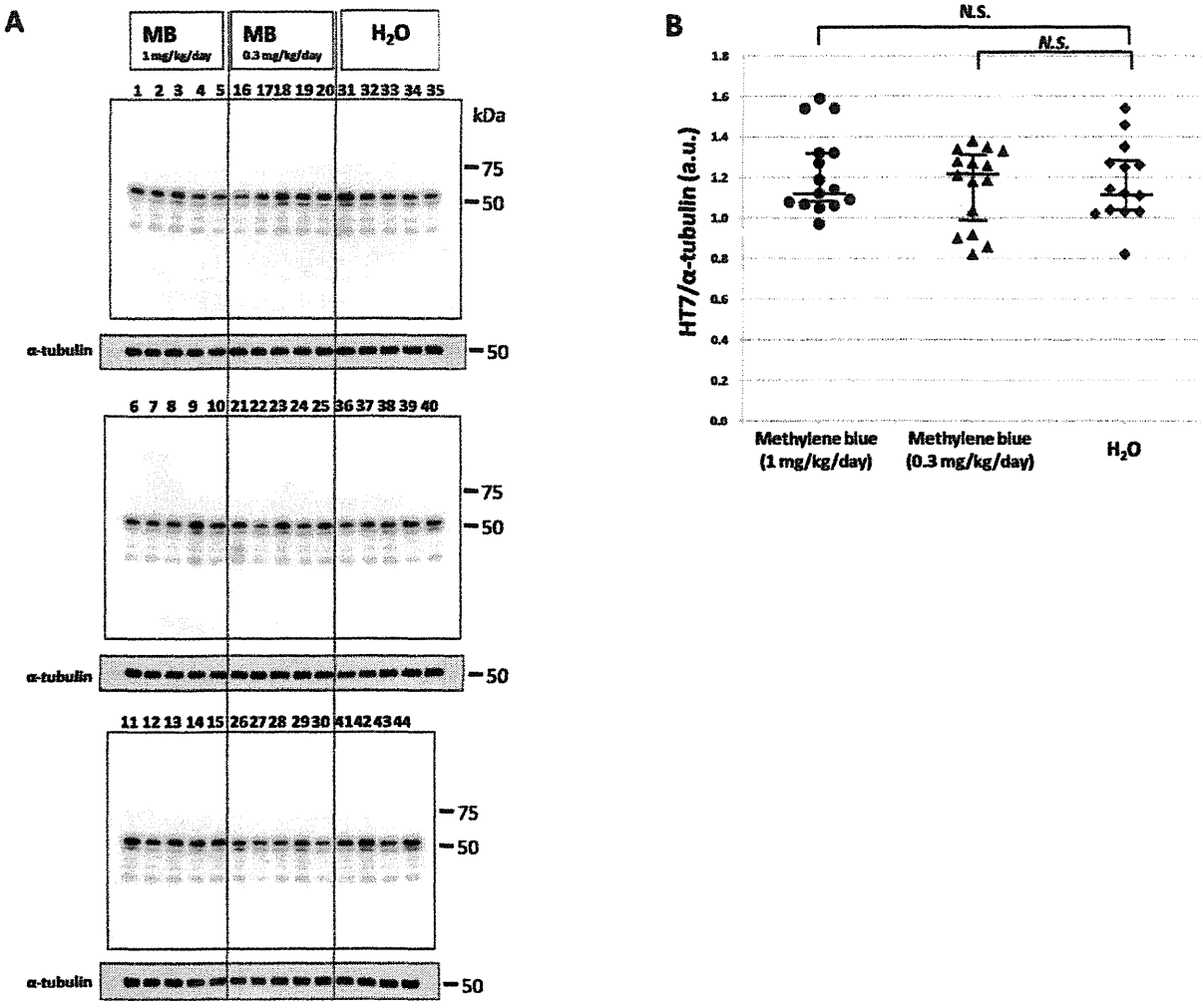

Figure 1. Immunoblotting analysis of total tau in the Tris-soluble fraction. (A) Immunoblotting analysis was visualized using HT7 antibody for the Tris-soluble fraction. The numbers indicate individual mice: 1–15, MB 1 mg/kg/day group; 16–30, MB 0.3 mg/kg/day group; and 31–44, water only group. Molecular weight markers are shown on the right (kDa). For quantitative measure of band intensity, α-tubulin was used as an internal control for protein concentration. (B) A comparison of the relative total tau (HT7) expression levels of the MB-treated groups and the water only group. The data were compared with the HT7 band intensity, which was normalized with α-tubulin. The central lines indicate medians and the vertical lines represent 25th and 75th percentiles. a.u., arbitrary unit. N.S., no significant difference.
doi:10.1371/journal.pone.0052389.g001

Animals

P301L tau transgenic mice (JNPL3) [8] were purchased from Taconic (USA) via IBL (Japan). The experiments utilized 44 female hemizygote tau mice. The mice were reared in the animal facility of Tokyo Metropolitan Institute of Medical Science under standard conditions at 24±2°C and were maintained on a commercial diet supplied ad libitum.

The transgenic mice [8] aged 8–11 months were divided into 3 groups: the first group (14 mice) was given water alone, the second group (15 mice) was given water containing 2 μg/ml MB and the third group (15 mice) was given water containing 6 μg/ml MB. All were maintained on their respective regimens for 5 months. The daily MB intake was estimated to be about 0.3 or 1 mg/kg/day per mouse, on the assumption that a mouse weighs 30 g and takes in 5 ml of water a day.

At the end of the experimental period, mice were sacrificed under quick anesthesia with 200 mg/kg body weight of sodium pentobarbital delivered intraperitoneally and their brains were quickly removed. Brains of each group were cut along the sagittal plane and the left hemisphere was frozen and stored at −80°C for biochemical analyses. The right hemisphere was fixed in 4% paraformaldehyde in 0.1 M phosphate buffer for 48 hours in the cold. Brain blocks were then transferred to a maintenance solution of 15% sucrose in 0.01 M phosphate-buffered saline (PBS), pH 7.4.

Analysis of Tau Deposition

Deposition of tau was analyzed using immunohistochemical staining with AT8 antibody (recognizes phosphorylation at both serine 202 and threonine 205) and MC-1 antibody. Biotinylation of MC-1 antibody was performed using a Zenon Mouse IgG

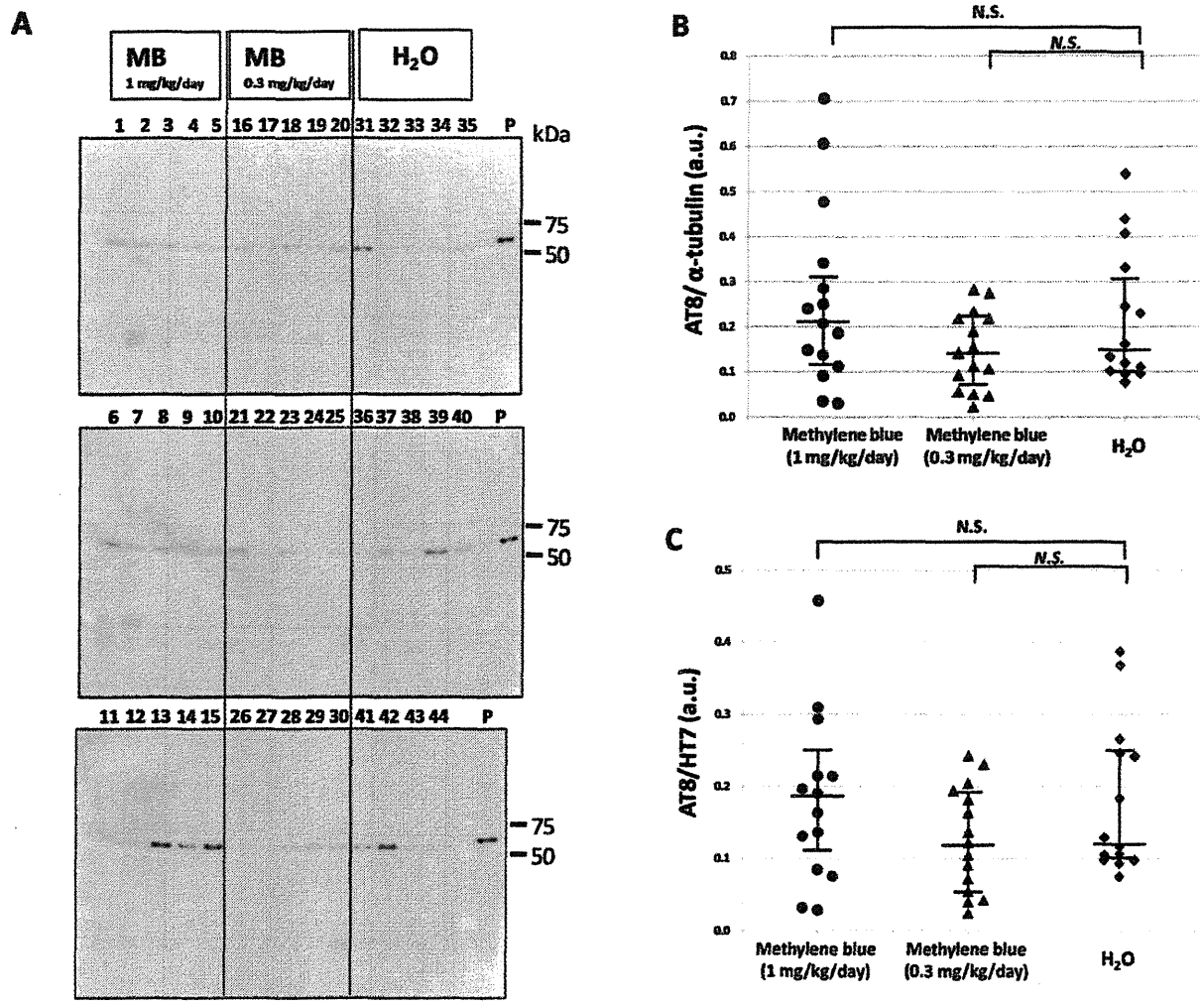

Figure 2. Immunoblotting analysis of phosphorylated tau in the Tris-soluble fraction. *(A) Immunoblot analysis was visualized using* AT8 antibody for the Tris-soluble fraction. The numbers indicate individual mice: 1–15, MB 1 mg/kg/day group; 16–30, MB 0.3 mg/kg/day group; and 31–44, water only group. Molecular weight markers are shown on the right (kDa). P, positive control (P301L tau transgenic mouse, 20 month-old female). (B) A comparison of relative phosphorylated tau (AT8) expression levels of the MB-treated groups and the water only group. The data were compared with the AT8 band intensity, which was normalized with α-tubulin. (C) A comparison of the relative phosphorylated tau (AT8)/total tau (HT7) levels of the MB-treated groups and the water only group. The data were compared with the AT8 band intensity, which was normalized with the total tau (HT7) band intensity. The central lines indicate medians and the vertical lines represent 25th and 75th percentiles. a.u., arbitrary unit. N.S., no significant difference.

doi:10.1371/journal.pone.0052389.g002

Labeling Kit (Molecular Probes, Inc. Eugene, OR, USA) according to the manufacturer's instructions. For immunohistochemistry, sagittal sections were cut serially on a freezing microtome at 30 μm thickness, collected in the maintenance solution, and immunostained as free-floating sections. Following a pretreatment with 0.5% H_2O_2 for 30 min to eliminate endogenous peroxidase activity, sections were incubated for 72 hours with AT8 antibody (Biotinylated-AT8, 1:1,000, Innogenetics, Ghent, Belgium) or overnight with biotinylated MC-1 antibody (1:100, a generous gift of Dr. Davies) [9] diluted in PBS containing 0.3% Triton X-100 (PBS-Tx). The antibody labeling was visualized by incubation with avidin-biotinylated horseradish peroxidase (HRP) complex (ABC Elite, 1:1,000, Vector Laboratories, Burlingame, CA, USA) for 3 hours, followed by incubation with a solution containing 0.01% 3,3′-diaminobenzidine (DAB), 1% nickel ammonium sulfate, 0.05 M imidazole and 0.00015% H_2O_2 in 0.05 M Tris-HCl buffer, pH 7.6. Counter nuclear staining was performed with Kernechtrot stain solution (Merck, Darmstadt, Germany). The sections were then rinsed with distilled water, mounted on glass slides, treated with Xylene, and coverslipped with Entellan (Merck). Photographs were taken with an Olympus VS120-S5 (Olympus, Tokyo, Japan) or a BX51 microscope (Olympus).

Sequential Fractionation of Brain Extracts

Frozen left hemispheres (approximately, 0.2 g) were homogenized in 10 volumes of buffer H (10 mM Tris-HCl, pH 7.5, 0.8 M NaCl, 1 mM ethylene glycol bis-N, N, N', N'-tetraacetic acid, 1 mM dithiothreitol). The hemisphere included the olfactory bulb, cerebral cortex, striatum, thalamus, hypothalamus, cerebellum,